This version of the ESI replaces the one published on 11.11.2022 to correct some errors in the upconversion data provided.

Electronic supporting information for:

Extracting accurate information from triplet-triplet annihilation upconversion data with a mass-conserving kinetic model

Abhishek Kalpattu,[a] Tristan Dilbeck,[b] Kenneth Hanson,[b] and John T. Fourkas*[c,d,e]

[a]Department of Materials Science and Engineering, University of Maryland, College Park, MD 20817, USA

[b]Department of Chemistry and Biochemistry, Florida State University, Tallahassee, FL 32306 USA

[c]Department of Chemistry and Biochemistry, University of Maryland, College Park, MD 20817, USA

[d]Institute for Physical Science and Technology, University of Maryland, College Park, MD 20817, USA

[e]Maryland Quantum Materials Center, University of Maryland, College Park, MD 20817, USA

*To whom correspondence should be addressed, fourkas@umd.edu

Table of Contents

The complete mass-conserving quartic model

The quartic model is derived by considering the effects of annihilator species conservation while determining the rate of triplet sensitization ($k_{sens}[^3S^*]_{SS}[A]_{SS}$). This model is given by the solution to the following expression for $[^3A^*]_{SS}$:

$$\frac{\mathrm{B}_{ISC}k_{sens}k_{ex}I[S]_0}{\mathrm{B}_{ISC}k_{ex}I + k_{sens}\left([A]_0 - [^3A^*]_{ss} - \frac{0.25(1+\beta_{RISC})k_{TTA}[^3A^*]_{SS}^2}{k_{fl}+k_{NR}^A+k_{ISC}'} - \frac{0.75k_{TTA}[^3A^*]_{SS}^2}{k_{IC}+k_{RISC}}\right) + k_T^S}$$
$$\left([A]_0 - [^3A^*]_{SS} - \frac{0.25(1+\beta_{RISC})k_{TTA}[^3A^*]_{SS}^2}{k_{fl}+k_{NR}^A+k_{ISC}'} - \frac{0.75k_{TTA}[^3A^*]_{SS}^2}{k_{IC}+k_{RISC}}\right) = k_T^A[^3A^*]_{SS}$$
$$+ 1.25(1+\beta_{RISC})k_{TTA}[^3A^*]_{SS}^2 - k_{ISC}'\frac{0.25(1+\beta_{RISC})k_{TTA}[^3A^*]_{SS}^2}{k_{fl}+k_{NR}^A+k_{ISC}'} \quad \text{(S1)}$$

Rearranging leads to:

$$\alpha_1[^3A^*]_{SS}^4 + \alpha_2[^3A^*]_{SS}^3 + \alpha_3[^3A^*]_{SS}^2 + \alpha_4[^3A^*]_{SS} + \alpha_5 = 0\,, \quad \text{(S2)}$$

where

$$\alpha_1 = k_{sens}\left(k_{ISC}{}'\frac{0.25(1+\beta_{RISC})k_{TTA}}{k_{fl}+k_{NR}^{A}+k_{ISC}{}'} - 1.25(1+\beta_{RISC})k_{TTA}\right)\left(\frac{0.25(1+\beta_{RISC})k_{TTA}}{k_{fl}+k_{NR}^{A}+k_{ISC}{}'} + \frac{0.75k_{TTA}}{k_{IC}+k_{RISC}}\right) \quad \text{(S3)}$$

$$\alpha_2 = -k_T^A k_{sens}\left(\frac{0.25(1+\beta_{RISC})k_{TTA}}{k_{fl}+k_{NR}^{A}+k_{ISC}{}'} + \frac{0.75k_{TTA}}{k_{IC}+k_{RISC}}\right) + k_{sens}\left(k_{ISC}{}'\frac{0.25(1+\beta_{RISC})k_{TTA}}{k_{fl}+k_{NR}^{A}+k_{ISC}{}'} - 1.25(1 \quad \text{(S4)}$$

$$\alpha_3 = -k_T^A k_{sens} + \left(k_{sens}[A]_0 + \mathrm{B}_{ISC}k_{ex}I + k_T^S\right)\left(k_{ISC}{}'\frac{0.25(1+\beta_{RISC})k_{TTA}}{k_{fl}+k_{NR}^{A}+k_{ISC}{}'} - 1.25(1+\beta_{RISC})k_{TTA}\right) I[S]_0\left(\frac{0.25(1+\beta_{RISC})k_{TTA}}{k_{fl}+k_{NR}^{A}+k_{ISC}{}'} + \frac{0.75k_{TTA}}{k_{IC}+k_{RISC}}\right) \quad \text{(S5)}$$

$$\alpha_4 = \mathrm{B}_{ISC}k_{sens}k_{ex}I[S]_0 + k_T^A\left(k_{sens}[A]_0 + \mathrm{B}_{ISC}k_{ex}I + k_T^S\right) \quad \text{(S6)}$$

and

$$\alpha_5 = -\mathrm{B}_{ISC}k_{sens}k_{ex}I[S]_0[A]_0 . \quad \text{(S7)}$$

The general solution to eqn (S2) is cumbersome, but can be represented as:

$$[{}^3A^*]_{SS} = \frac{-\alpha_2}{4\alpha_1} + S + \frac{\sqrt{-4S^2 - 2p - \frac{q}{S}}}{2}, \quad \text{(S8)}$$

where

$$S = \frac{1}{2}\sqrt{-\frac{2}{3}p + \left(\frac{1}{3\alpha_1}\left(Q + \frac{\Delta D_0}{Q}\right)\right)} \quad \text{(S9)}$$

$$Q = \sqrt[3]{\frac{\Delta D_1 + \sqrt{\left(\Delta D_1{}^2 - 4\Delta D_0{}^3\right)}}{2}} \quad \text{(S10)}$$

$$\Delta D_0 = \alpha_3{}^2 - 3\alpha_2\alpha_4 + 12\alpha_1\alpha_5 \quad \text{(S11)}$$

$$\Delta D_1 = 2\alpha_3{}^3 - 9\alpha_2\alpha_3\alpha_4 + 27\alpha_2{}^2\alpha_5 + 27\alpha_1\alpha_4{}^2 - 72\alpha_1\alpha_3\alpha_5 \tag{S12}$$

$$q = \frac{\alpha_2{}^3 - 4\alpha_1\alpha_2\alpha_3 + 8\alpha_1{}^2\alpha_4}{8\alpha_1{}^3} \tag{S13}$$

and

$$p = \frac{8\alpha_1\alpha_3 - 3\alpha_2{}^2}{8\alpha_1{}^2} . \tag{S14}$$

Note that eqn (S8) represents the only real and positive root to eqn (S2), so the other three solutions are not given here. When the expressions for S, Q, p, q, ΔD_0, ΔD_1, and α_1 through α_5 are substituted into eqn (S8), we obtain a complete solution for the steady-state concentration of annihilator triplets, which can then be used to obtain the steady-state rate of fluorescence under our complete mass-conserving model through

$$F_{SS} = \frac{k_{fl}(1+\beta_{RISC})0.25k_{TTA}[^3A]_{SS}^2}{k_{fl} + k_{NR}^{A} + k_{ISC}'} . \tag{S15}$$

Exploring the effects of sensitizer TTA

$[^1S^*]$, and $[^3S^*]$ at steady state can be described as

$$[^1S^*]_{SS} = \frac{k_{ex}I[S]_0}{k_{ex}I + k_{NR}{}^S + k_{ISC}} \tag{S16}$$

$$[^3S^*]_{SS} = \frac{B_{ISC}k_{ex}I[S]_0}{B_{ISC}k_{ex}I + k_{sens}[A] + k_T{}^S} \tag{S17}$$

To introduce and model the effects of sensitizer TTA, eqn (1) and eqn (2) in the main text can be modified to read

$$\frac{d[^1S^*]}{dt} = k_{ex}I[S] - k_{NR}^{S}[^1S^*] - k_{ISC}[^1S^*] + 0.25k_{TTA}^{S}[^3S^*]^2 \quad \text{(S18)}$$

and

$$\frac{d[^3S]}{dt} = k_{ISC}[^1S^*] - k_{sens}[^3S^*][A] - k_T^S[^3S^*] - 1.25k_{TTA}^{S}[^3S^*]^2 . \quad \text{(S19)}$$

Note that the coefficients in front of the $k_{TTA}^{S}[^3S^*]^2$ terms originate from spin statistics. Here, IC from higher-order sensitizer triplet states is not considered explicitly. At steady-state, eqn (S19) can be expressed as

$$k_{TTA}^{S}[^3S^*]_{SS}^2(1.25 + 0.25B_{ISC})[^3S^*]^2(1.25 - 0.25B_{ISC}) +$$

$$k_{sens}[^3S^*]_{SS}[A] + k_T^S[^3S^*]_{SS} + B_{ISC}k_{ex}I[^3S^*]_{SS} = B_{ISC}k_{ex}I[S]_0 \quad \text{(S20)}$$

Eqn (20) can be solved to obtain

$$[^3S^*]_{SS} = \frac{-\left(k_{sens}[A]_{SS} + k_{ex}I + k_T^S\right) - \sqrt{\left(k_{sens}[A]_{SS} + B_{ISC}k_{ex}I + k_T^S\right)^2 + 4k_{TTA}^{S}B_{ISC}k_{ex}}}{2k_{TTA}^{S}} \quad \text{(S21)}$$

$[^3S^*]_{SS}$ can be substituted into the following to obtain $[^3A^*]_{SS}$:

$$[^3S^*]_{SS}\left([A]_0 - [^3A^*]_{SS} - \frac{0.25(1+\beta_{RISC})k_{TTA}[^3A^*]_{SS}^2}{k_{fl} + k_{NR}^{A} + k_{ISC}'} - \frac{0.75k_{TTA}[^3A^*]_{SS}^2}{k_{IC} + k_{RISC}}\right)$$

$$= k_T^A[^3A^*]_{SS} + 1.25(1+\beta_{RISC})k_{TTA}[^3A^*]_{SS}^2 - k_{ISC}'\frac{0.25(1+\beta_{RISC})k_{TTA}[^3A^*]_{SS}^2}{k_{fl} + k_{NR}^{A} + k_{ISC}'} \quad \text{(S22)}$$

Finally, F_{SS} can be obtained by substituting the solution to eqn (S22) into eqn (S15). Note that a general solution to eqn (S22) for $[^3A^*]$ cannot be obtained unless the assumption is made that $[A]_{SS} \cong [A]_0$. However, numerical solutions of eqn (S22) show that the effect of making such an approximation is negligible under conditions in which sensitizer TTA becomes influential (See Figs. S1c and S1d).

Figs. S1a and S1b explore the importance of sensitizer TTA (see Table S2 for the parameters used in this figure). When k_{sens} is large, sensitizer TTA has no discernable effect on the rate of upconverted fluorescence. Typically, $[A]$ is several orders of magnitude larger than $[^3S^*]$. Therefore the rate of sensitizer TTA, which is proportional to $[^3S^*]^2$, is generally negligible when compared to the rate of triplet sensitization, which is proportional to $[^3S^*][A]$. Fig. S1b illustrates how sensitizer TTA starts to limit the rate of upconverted fluorescence appreciably only when k_{sens} is several orders smaller than k_{TTA}^{S}. Only in the unrealistic situation in which k_{sens} is three orders of magnitude smaller than k_{TTA}^{S} and $[S]_0$ is an order of magnitude less than $[A]_0$ do the effects of sensitizer TTA become begin to become apparent (Fig. S1b). In the examples shown in Fig. S1a and S1b, the TTA rate constants are roughly an order of magnitude smaller than k_{sens}. Even when these three rate constants are of the same magnitude, the effects of sensitizer TTA continue to be negligible (not shown).

Figs. S1c demonstrates that both the quadratic and quartic models give virtually identical predictions when sensitizer TTA is present. Even when k_{TTA} is nearly five orders of magnitude smaller than k_{sens}, these two models differ only slightly, near the saturation regime. Furthermore, as shown in Fig. S1d, in the quartic model with a unrealistically small value of k_{TTA}, sensitizer TTA makes no difference in a logarithmic plot of the fluorescence rate vs. the irradiance.

Because sensitizer TTA offers a competitive pathway to eliminate sensitizer triplets for certain TTA-UC systems, complete saturation of upconverted fluorescence would be observed at much higher irradiances than in cases where sensitizer TTA is not prevalent. At high enough irradiances, F_{SS} first develops a square root dependence on I, before complete saturation occurs. Despite the delayed onset of complete saturation, sensitizer TTA always leads to reduced rates of upconverted fluorescence, and is therefore detrimental to Φ_{UC}. Although the results of sensitizer TTA are interesting, and deserving of a deeper study with our mass conserving TTA-UC model, the results presented here make it clear that there are few circumstances in which is necessary to incorporate sensitizer TTA in the analysis of TTA plots of the type discussed here.

Deriving the characteristics of a simple TTA-UC model

Many of the characteristics of the TTA-UC process in our model can be understood by simplification of the expression

$$\frac{\mathrm{B}_{ISC}k_{sens}k_{ex}I[S]_0}{\mathrm{B}_{ISC}k_{ex}I + k_{sens}[A]_{SS} + k_T^S}\left([A]_0 - [^3A^*]_{ss} - \frac{0.25(1+\beta_{RISC})k_{TTA}[^3A^*]_{SS}^2}{k_{fl} + k_{NR}^A + k_{ISC}'} - \frac{0.75k_{TTA}[^3A^*]_{SS}^2}{k_{IC} + k_{RISC}}\right)$$

$$= k_T^A[^3A^*]_{ss} + 1.25(1+\beta_{RISC})k_{TTA}[^3A^*]_{SS}^2 - k_{ISC}'\frac{0.25k_{TTA}[^3A^*]_{SS}^2}{k_{fl} + k_{NR}^A + k_{ISC}'} \quad \text{(S23)}$$

We begin by considering the classic irradiance limits of TTA-UC and the expression for the irradiance at which the extrapolated limiting behaviors are equal, which is commonly denoted I_{th}. For an ideal TTA-UC system, an expression for I_{th} that is derived without the consideration of mass conservation will closely resemble the expression for I_{th} from our mass-conserving

model. To show this result, we consider a simplified version of eqn (S23) in which we assume that $\beta_{RISC} = 0$, $k_{ISC}' = 0$, $B_{ISC} = 1$, and $k_{sens}[A]_{SS} \cong k_{sens}[A]_0$:

$$\frac{k_{sens}k_{ex}I[S]_0}{k_{ex}I + k_{sens}[A]_0 + k_T^S}\left([A]_0 - [^3A^*]_{ss} - \frac{0.25k_{TT}[^3A^*]_{SS}^2}{k_{fl} + k_{NR}^A} - \frac{0.75k_{TT}[^3A^*]_{SS}^2}{k_{IC}}\right)$$

$$= k_T^A[^3A^*]_{ss} + 1.25k_{TT}[^3A^*]_{SS}^2 . \quad \text{(S24)}$$

The $k_{ex}I$ term in the denominator of the left-hand side of eqn (S24) arises from the implementation of mass conservation in obtaining the steady-state concentration of sensitizer triplets. If we were instead to assume that the concentration of sensitizer triplets is much lower than the initial concentration of sensitizers, then $[S]_{ss}$ can be approximated as $[S]_0$. In this case, sensitizer mass conservation is ignored. Similarly, the second term in parentheses arises from mass conservation in the annihilator, and is negligible when $[A]_0 \gg [^3A^*]_{SS}$. We can therefore re-express eqn (S24) as

$$\beta_{sens}k_{ex}I[S]_0 = [^3A^*]_{SS}k_T^A + 1.25k_{TTA}[^3A^*]_{SS}^2 . \quad \text{(S25)}$$

When the irradiance is small enough, the $[^3A^*]_{SS}^2$ term is negligibly small, such that we can describe steady-state fluorescence in the low-irradiance regime as

$$F_{SS,low} = 0.25\Phi_{fl}k_{TTA}[^3A^*]_{SS}^2 = 0.25\Phi_{fl}k_{TTA}\left(\frac{\beta_{sens}k_{ex}I[S]_0}{k_T^A}\right)^2 . \quad \text{(S26)}$$

Thus, the steady-state fluorescence scales as I^2 at low enough irradiance. Given the conditions that had to be met to reach eqn (S26), it is clear that the irradiance must generally be quite low to attain this limit. This fact is not often discussed in the TTA-UC literature, but has important ramifications for the experimental determination of I_{th}.

At high irradiance, we can assume that the terms in eqn (S24) that are linear in $[^3A]_{ss}$ are unimportant, yielding

$$\beta_{sens} k_{ex} I[S]_0 = 1.25 k_{TTA} [^3A^*]_{SS}^2 . \quad \text{(S27)}$$

Therefore, the rate of steady-state fluorescence at the high irradiance limit may be expressed as

$$F_{SS,high} = 0.25 \Phi_{fl} k_{TTA} [^3A^*]_{SS}^2 = \frac{\Phi_{fl} \beta_{sens} k_{ex} I[S]_0}{5} . \quad \text{(S28)}$$

We find I_{th} by setting eqn (S28) equal to eqn (S26) and solving for the irradiance:

$$I_{th} = \frac{\left(k_T^A\right)^2}{1.25 \beta_{sens} k_{ex} k_{TTA} [S]_0} . \quad \text{(S29)}$$

In deriving our expression for I_{th}, we have ignored the effects of mass conservation by replacing the steady-state concentrations of sensitizers and annihilators with their initial concentrations.

Analyzing differences in saturation behavior between the quartic and quadratic models

As discussed in the main text, the quartic and quadratic models deviate most appreciably near saturation. The difference between the two models is that the steady-state concentration of sensitizer triplets in the quartic model is implicitly dependent on the steady-state concentrations of excited annihilator molecules through $[A]_{SS}$. In the quadratic model, the steady-state concentration of sensitizer triplets is dependent only on $[A]_0$, which is a constant. However, the overall rate of sensitization, R_{sens}, still retains a dependence on $[A]_{SS}$ under the quadratic approximation. A result of the substitution of $[A]_{SS}$ with $[A]_0$ in the quadratic model is that as

$[A]_{SS}\rightarrow 0$, the rate of sensitization in the quadratic model drops more quickly than that in the quartic model. Ultimately, however, the saturation rate of fluorescence, $F_{SS,\,sat}$, is identical in both models. Hence, saturation occurs more rapidly and at lower irradiances in the quartic model, resulting in smaller I_{sat} values. On the other hand, Γ is larger in the quartic model under some conditions. Fig. S3b shows that the discrepancy in I_{sat} between the two models is larger when k_{TTA} is small. Lower values of $[A]_0/[S]_0$ further exacerbate these discrepancies, as the approximation that $[A]_{SS} = [A]_0$ becomes invalid under these conditions. Interestingly, the trend in the discrepancies in Γ between the two models is not monotonic, unlike that for the discrepancies in I_{sat}. In Fig. S3c, the quantity $\Gamma_{quartic} - \Gamma_{quadratic}$ is plotted as a function of k_{TTA} for different values of $[A]_0$ and $[S]_0$. When k_{TTA} is small enough that the irradiance at which efficient TTA is expected is much larger than the irradiance at which $[A]_{SS}\rightarrow 0$, Γ is larger in the quadratic model than in the quartic model. This behavior arises from the fact that the quadratic model exhibits a smoother transition in local slope, from a value of 1 to a value of 0, with increasing irradiance. On the other hand, under the quartic model, the local slope drops from a value of ~1 to 0 almost instantly once $[A]_{SS}\rightarrow 0$. The smooth transition that is predicted by the quadratic model, results in a larger Γ. When k_{TTA} is increased, this effect vanishes, and the discrepancy in Γ increases in favor of the quartic model. Due to the inherent uncertainty in determining $I_{0.9}$ and $I_{1.1}$ for the quartic model at low k_{TTA}, $\Gamma_{quartic} - \Gamma_{quadratic}$ values for $k_{TTA} < 1 \times 10^5\ M^{-1}s^{-1}$ are omitted from Fig. S3c. Once k_{TTA} is large enough, however, another form of saturation is achieved, i.e. the condition $k_{ex}I > k_{sens}[A]_{SS}$ is satisfied, before $[A]_{SS}$ is allowed to reach 0. This phenomenon explains why the difference in Γ between the two models begins to drop once more, finally settling at 0. The discrepancy in Γ values is more pronounced in systems with lower $[A]_0/[S]_0$.

Exploring deviations in the transition width Γ for specific values of k_{TTA} and $[A]_0$

In specific cases, the relationship between Γ and k_{TTA} or $[A]_0$ is nonlinear, which would not be expected given our basic analysis based on the transition width $\log(I_{sat}/I_{th})$. In Fig. S6, we see that within the region between the dotted lines, the relationship between Γ and k_{TTA} is different than that at higher values of k_{TTA}. Specifically, we find that $\Gamma \propto (k_{TTA})^{1.6}$ within this region. When k_{TTA} is small, the TTA-UC process can never proceed efficiently, because at the values of irradiances at which the TTA process would become more dominant than the intrinsic triplet quenching mechanism, fluorescence saturation starts to occur. However, as k_{TTA} is increased, not only is the irradiance at which the TTA-UC process becomes efficient reduced, but the irradiance at which saturation occurs increases, because the rate at which annihilator states are made available for triplet sensitization increases. A similar observation can be made with respect to Γ and $[A]_0$. The latter observation can be explained by use of the quantity $\log(I_{sat}/I_{th})$. In the quadratic model, I_{sat} always increases with increasing $[A]_0$, because the steady-state concentration of annihilators in the ground state is assumed to be $[A]_0$ for the purposes of determining the rate of triplet sensitization. On the other hand, when $[A]_0$ is small, the sensitization branching ratio β_{sens} is less than 1, and so I_{th}, which is inversely proportional to β_{sens}, decreases as $[A]_0$ increases. The simultaneous decrease in I_{th} and increase in I_{sat} lead to a nonlinear growth in Γ with $[A]_0$.

The origin of saturation in the quadratic model

As mentioned in the main text, in the quadratic model fluorescence saturation arises primarily due to the effects of sensitizer mass conservation. Because $[A]_0$ is typically much larger than

$[^3A^*]_{ss}$, we rarely encounter cases in which the accumulation of annihilator triplets stifles any growth in the rate of triplet sensitization, as was seen in the comparison of the quartic and quadratic models. In Fig. S2 we plot $[^3A^*]_{SS}$ for a range of system parameters. These plots reveal that only when the rate of triplet sensitization is on the order of 10^{13} $M^{-1}s^{-1}$ does $[^3A^*]_{SS}$ approach $[A]_0$. In this situation, the term within the brackets of eqn (S24) drops almost to 0, thus removing the dependence of $[^3A^*]_{SS}$ on *I*.

Expanding and analyzing the expression for *n*(*I*) from the kinetic model

Recall that *n*(*I*) is derived from

$$\frac{d(\log(F_{ss}))}{d(\log(I))} = \frac{d(\log(F_{ss}))}{dF_{ss}} \Big/ \frac{d(\log(I))}{dI} = \frac{I}{F_{ss}} \cdot \frac{dF_{ss}}{dI} . \tag{S30}$$

To evaluate this derivative analytically in a facile manner, we represent the solution to eqn (S24) as

$$[^3A^*]_{SS} = \frac{c_1 I + c_2}{c_3 I + c_4}\left(\sqrt{1 + \frac{c_5 I^2 + c_6 I}{c_7 I^2 + c_8 I + c_9}} - 1\right), \tag{S31}$$

where

$$c_1 = k_T^A k_{ex} + k_{sens} k_{ex} [S]_0 \left(\left(k_{fl} + k_{NR}^A\right) k_{IC}\right) \tag{S32}$$

$$c_2 = k_T^A \left(k_{sens} [A]_0 + k_T^S\right) \tag{S33}$$

$$c_3 = 2.5 k_{TTA} k_{ex} \left(k_{fl} + k_{NR}\right) k_{IC} + k_{sens} k_{ex} [S]_0 (0.25 k_{IC} + 2\left(k_{fl} + k_{NR}^A\right) \tag{S34}$$

$$c_4 = k_T^A k_{IC} \left(k_{sens} [A]_0 + k_T^S\right)\left(k_{fl} + k_{NR}^A\right) \tag{S35}$$

$$c_5 = 5k_{sens}k_{TTA}{k_{ex}}^2[S]_0[A]_0\left(k_{fl} + k_{NR}^A\right)k_{IC} \tag{S36}$$

$$c_6 = 4k_{sens}k_{ex}k_{TT}[S]_0[A]_0k_{IC}\left(k_{sens}[A]_0 + k_T^S\right)\left(k_{fl} + k_{NR}^A\right)$$

$$+ k_{sens}k_{ex}I[S]_0(0.25k_{IC} + 2\left(k_{fl} + k_{NR}^A\right) \tag{S37}$$

$$c_7 = k_T^Ak_{ex}k_{sens}k_{ex}[S]_0\left(k_{fl} + k_{NR}^A\right)k_{IC} \tag{S38}$$

$$c_8 = 2k_T^Ak_{sens}k_{ex}[S]_0\left(k_{sens}[A]_0 + k_T^S\right)\left(k_{fl} + k_{NR}^A\right)k_{IC} \tag{S39}$$

and

$$c_9 = \left(k_T^A\left(k_{sens}[A]_0 + k_T^S\right)\right)^2\left(k_{fl} + k_{NR}^A\right)k_{IC} \ . \tag{S40}$$

The local slope $n(I)$ can then be expressed as

$$n(I) = I\left(\frac{\left(\frac{c_5c_8I^2 + 2c_5c_9I - c_6c_7I^2 + c_6c_9}{\left(c_7I^2 + c_8I + c_9\right)^2}\right)}{\left(\sqrt{1 + \frac{c_5I^2 + c_6I}{c_7I^2 + c_8I + c_9}} - 1\right)\sqrt{1 + \frac{c_5I^2 + c_6I}{c_7I^2 + c_8I + c_9}}} + 2\frac{c_1c_4 - c_2c_3}{(c_1I + c_2)(c_3I + c_4)}\right) . \tag{S41}$$

In the limit in which I is small, eqn (S41) reduces to

$$n(I) = \frac{\frac{c_6}{c_9}I}{\sqrt{1 + \frac{c_6I}{c_9}} - 1} + 2I\frac{(c_1c_4 - c_2c_3)}{c_2c_4} \ . \tag{S42}$$

If the second term in the radicand is much less than 1, this expression becomes

$$n(I) = \frac{\frac{c_6}{c_9}I}{\frac{c_6 I}{2c_9}} + 2I\frac{(c_1c_4 - c_2c_3)}{c_2c_4} = 2 + 2I\frac{(c_1c_4 - c_2c_3)}{c_2c_4} \cong 2 \quad . \tag{S43}$$

Therefore, at low enough irradiance, the local slope is 2, as expected. At a high enough irradiance, it must be the case that $\sqrt{1 + \frac{c_5I^2 + c_6I}{c_7I^2 + c_8I + c_9}} \gg 1$, and so eqn (S41) becomes

$$n(I) = I\left(\frac{c_5c_8I^2 + 2c_5c_9I - c_6c_7I^2 + c_6c_9}{\left(c_7I^2 + c_8I + c_9\right)\left(c_7I^2 + c_8I + c_9 + c_5I^2 + c_6I\right)} + 2\frac{c_1c_4 - c_2c_3}{(c_1I + c_2)(c_3I + c_4)}\right). \tag{S44}$$

The irradiance at which the local slope attains a value of 1 can be calculated from eqn (S44). Because eqn (S44) is a 6th-order polynomial in *I*, a general solution for *I* at *n* = 1 cannot be found. However, in the limit in which *I* is large enough that the quadratic terms dominate eqn (S44), we find that

$$n(I) = \frac{c_5c_8 - c_6c_7}{\left(c_5 + c_7\right)c_7I} + 2\frac{c_1c_4 - c_2c_3}{c_1c_3I} \quad . \tag{S45}$$

Thus, $n(I) \to 0$ in the limit that $I \to \infty$.

Dependence of $\bar{\Phi}_{UC}$ on *n*(*I*)

We showed in the main text that, by definition, $\bar{\Phi}_{UC}$ attains a value of 1 when *n* = 1. Fig. S8 shows that as k_{TTA} is increased and k_T^A is decreased, $\bar{\Phi}_{UC}$ increases smoothly with *n*. A representative plot of $\bar{\Phi}_{UC}$ vs. *n*, from which we had obtained our inverse exponential relationship between $\bar{\Phi}_{UC}$ and *n*, is shown in Fig. S9.

Exploring the influence of k_{TTA} and k_T^A on $[^3A^*]_{SS}$

We found in the main text that under a typical scenario in which k_{TTA} is large and k_T^A is small, k_{TTA} and k_T^A have negligible impact on the steady-state rate of fluorescence at high irradiance. However, this situation need not hold under atypical TTA-UC conditions, in which $\Phi_{UC,max}$ and I_{sat} may depend on k_{TTA} and k_T^A. To illustrate this behavior, we consider the second term within the radicand of eqn (S31), ρ. Figure S10 shows that under ideal conditions, ρ is maximized at low irradiance at which saturation does not occur. However, under nonideal conditions, ρ is only ever maximized at high irradiance, and often at its saturation value, at which $k_{ex}I > k_{sens}[A]_0$. Note that only when $\rho \gg 1$ does the rate of fluorescence at high irradiances become completely independent of k_{TTA} and k_T^A. Therefore, when ρ peaks at smaller values and at higher irradiances, k_{TTA} and k_T^A start to have an effect on $\Phi_{UC,max}$ and I_{sat}.

Fitting literature data on upconverted fluorescence from TTA-UC solutions

Typically, fluorescence intensities are reported in arbitrary units. Therefore, to facilitate the curve-fitting process, experimental fluorescence intensity data were normalized by dividing each data set by the highest value of fluorescence intensity measured in that data set. Representative quadratic fits of data from the literature are shown in Figs. S14, S15, and S17-S20.

The robustness of I_{th} to changes in fitting parameters

Although the combination of extracted system parameters from best fits to literature data may not be unique, the performance factors that are calculated from the two different sets of extracted rate parameters are nearly identical as long as both fits are equally good. In essence,

best fits to experimental data give insights into the ratios of rate parameters such as k_{TTA}, k_{ex}, and k_T^A. Because I_{th} is proportional to $\frac{(k_T^A)^2}{k_{TTA}k_{ex}}$, there are numerous different combinations of reasonable values of k_{TTA}, k_{ex}, and k_T^A that result in the same I_{th}. Because a small degree of uncertainty in fitting experimental data always exists (no experimental dataset can be fit perfectly), minor deviations in I_{th} will unavoidably arise when fitting constraints are modified. However, as we show below, the deviations in I_{th} that arise from an uncertainty in fitting, are only minor.

As an example, we fit experimental data from Ogawa *et al.*[1] to obtain a k_{TTA} of 3×10^9 M^{-1} s^{-1}, a k_T^A of 2039 s^{-1}, and a k_{ex} of 10.09 cm^2/mJ (See Table S1 for the other parameters). When we constrained k_{TTA} to a value of 3×10^8 $M^{-1}s^{-1}$ instead, k_T^A was reduced to 1894 s^{-1}, and a k_{ex} was increased to 85.7 cm^2/mJ (the other parameters did not change). The goodness of the fit improved slightly (R^2 = 0.9998 vs. 0.9997). Despite the change in parameters, the value of I_{th} obtained from the fit changed only from 11.0 mW/cm^2 to 11.1 mW/cm^2.

As another example, our fits to experimental data from Gray *et al.*[2], yielded an I_{th} of 33.02 mW/cm^2 with an extracted k_{TTA} of 3×10^9 M^{-1} s^{-1}, a k_T^A of 326.8 s^{-1}, and a k_{ex} of 0.0576 cm^2/mJ (See Table S1 for the other parameters). When k_{TTA} was constrained to be 3×10^8 M^{-1} s^{-1} instead, k_T^A was reduced to 245.6 s^{-1}, and k_{ex} was increased to 0.3239 cm^2/mJ (the other parameters did not change). The R^2 was identical in each case, and I_{th} changed to 33.16 mW/cm^2. Therefore, different combinations in rate parameters that are extracted from equally good fits to experimental data with our TTA-UC model do not result in significant changes to I_{th}.

Simulation and curve-fitting methodology (MATLAB)

MATLAB code that was used to generate logarithmic TTA-UC curves, compute expressions for $n(I)$ and corresponding $n(I)$ vs. I curves, calculate Φ_{UC} and $\Phi_{UC,max}$ values, and calculate Γ and many other system parameters is available via GitHub. Table S3 provides a summary description of the files found in the GitHub folder.

Curve-fitting toolbox and example

The curve-fitting toolbox can be accessed from the 'APPS' tab in MATLAB. With the toolbox opened, x-axis data (irradiance, not $log(I)$), and y-axis data (fluorescence output) should be loaded. An appropriate weighting scale should be applied to ensure that fluorescence emission values at low irradiances (which are exponentially smaller than those at high irradiances) will be considered equally in performing the fit. In our work, we use a weighting factor of $1/\overline{F}_{SS}(I)$, where $\overline{F}_{SS}(I)$ represents fluorescence output values that are normalized such that the highest possible value is 1. To begin the fitting process, the 'Custom Equation' option must be selected from the drop-down menu found at the top of the curve fitting toolbox. A custom quadratic model fitting equation, containing known system parameters as well unknown fitting parameters, can be generated using the Matlab code titled 'FittingShow.m' (See Table S3). The fitting equation should then be used to replace the default custom equation that appears at the top of curve fitting toolbox. Please note that the fitting variable should be changed from the default 'x' to 'I' for fitting to proceed. Following this step, one may open the 'fitting options' dialog box to enter guess values for the various rate constants and coefficients involved in the TTA-UC process, as well as to create specific upper/lower bounds. MATLAB should begin fitting automatically, and will update its best fit as new guess values are entered. Once a satisfactory fit is obtained (the goodness of any particular fit is given by the R^2 value which

Matlab provides in the toolbox), the obtained rate constants and system parameters can be copied for plotting with the code found in 'FssShow.m' (See Table. S3). Fig. S21 illustrates MATLAB's curve-fitting toolbox as TTA-UC data from a solution mixture of PtOEP and DPA is being fit.

References

1. T. Ogawa, N. Yanai, A. Monguzzi and N. Kimizuka, *Sci. Rep.*, 2015, **5**, 10882.
2. V. Gray, D. Dzebo, A. Lundin, J. Alborzpour, M. Abrahamsson, B. Albinsson and K. Moth-Poulsen, *J. Mater. Chem. C*, 2015, **3**, 11111-11121.
3. A. Olesund, V. Gray, J. Mårtensson and B. Albinsson, *J. Amer. Chem. Soc.*, 2021, **143**, 5745-5754.
4. V. Gray, A. Dreos, P. Erhart, B. Albinsson, K. Moth-Poulsen and M. Abrahamsson, *Phys. Chem. Chem. Phys.*, 2017, **19**, 10931-10939.
5. M. Han, Z. Zhu, M. Ouyang, Y. Liu and X. Shu, *Adv. Funct. Mater.*, 2021, **31**, 2104044.
6. D. Lin, J. Zhong, S. Ji, Z. Yuan, L. Xing, Q. He, H. Zhang and Y. Huo, *Dyes Pigm.*, 2021, **185**, 108912.
7. A. Haefele, J. Blumhoff, R. S. Khnayzer and F. N. Castellano, *J. Phys. Chem. Lett.*, 2012, **3**, 299-303.
8. A. Ronchi, P. Brazzo, M. Sassi, L. Beverina, J. Pedrini, F. Meinardi and A. Monguzzi, *Phys. Chem. Chem. Phys.*, 2019, **21**, 12353-12359.
9. S. Amemori, Y. Sasaki, N. Yanai and N. Kimizuka, *J. Amer. Chem. Soc.*, 2016, **138**, 8702-8705.
10. M. Wu, D. N. Congreve, M. W. B. Wilson, J. Jean, N. Geva, M. Welborn, T. Van Voorhis, V. Bulović, M. G. Bawendi and M. A. Baldo, *Nat. Photonics*, 2016, **10**, 31-34.
11. L. Nienhaus, J.-P. Correa-Baena, S. Wieghold, M. Einzinger, T.-A. Lin, K. E. Shulenberger, N. D. Klein, M. Wu, V. Bulović, T. Buonassisi, M. A. Baldo and M. G. Bawendi, *ACS Energy Lett.*, 2019, **4**, 888-895.

12. Y. Kawashima, H. Kouno, K. Orihashi, K. Nishimura, N. Yanai and N. Kimizuka, *Mol. Syst. Des. Eng.*, 2020, **5**, 792-796.

13. A. L. Hagstrom, H.-L. Lee, M.-S. Lee, H.-S. Choe, J. Jung, B.-G. Park, W.-S. Han, J.-S. Ko, J.-H. Kim and J.-H. Kim, *ACS Appl. Mater. Interfaces*, 2018, **10**, 8985-8992.

14. T.-A. Lin, C. F. Perkinson and M. A. Baldo, *Adv. Mater.*, 2020, **32**, 1908175.

15. Y. Zhou, S. Ayad, C. Ruchlin, V. Posey, S. P. Hill, Q. Wu and K. Hanson, *Phys. Chem. Chem. Phys.*, 2018, **20**, 20513-20524.

16. R. Vadrucci, A. Monguzzi, F. Saenz, B. D. Wilts, Y. C. Simon and C. Weder, *Adv. Mater.*, 2017, **29**, 1702992.

17. D. F. Barbosa de Mattos, A. Dreos, M. D. Johnstone, A. Runemark, C. Sauvée, V. Gray, K. Moth-Poulsen, H. Sundén and M. Abrahamsson, *J. Chem. Phys.*, 2020, **153**, 214705.

Table S1. Parameters used in figures in the main text and Supporting Information.

Figure	Parameters									
	k_{sens} ($M^{-1}s^{-1}$)	k_{TTA} ($M^{-1}s^{-1}$)	k_T^A (s^{-1})	k_{ex}* (cm^2/mJ)	$[S]_0$ (mM)	$[A]_0$ (mM)	k_{IC} (s^{-1})	k_{fl}* (s^{-1})	k_{NR}* (s^{-1})	k_{T*}^S (s^{-1})
2a	1.63×10^9	3.6×10^8	200	5	--	100	2×10^8	1.36×10^8	5.037×10^5	2×10^3
2b	1.63×10^9	3.6×10^4	200	5	--	100	2×10^8	1.36×10^8	5.037×10^5	2×10^3
3	1.63×10^9	3.6×10^8	200	5	0.014	100	2×10^8	1.36×10^8	5.037×10^5	2×10^3
4	1.63×10^9	3.6×10^8	200	5	0.014	100	2×10^8	1.36×10^8	5.037×10^5	2×10^3
5	1.63×10^9	3.6×10^8	200	5	0.014	100	2×10^8	1.36×10^8	5.037×10^5	2×10^3
6	1.63×10^9	3.6×10^8	200	5	0.014	100	2×10^8	1.36×10^8	5.037×10^5	2×10^3
7	1.63×10^8	3.6×10^9	2×10^4	5	0.014	1000	2×10^8	1.36×10^8	5.037×10^5	2×10^3
8a	2×10^9	2.8×10^8	1.1×10^4	44.7	0.05	1	2×10^8	2×10^8	4.8×10^{-1}	2×10^3
8b	2.3×10^9	2.5×10^8	1.2×10^5	725	0.075	0.091	2×10^8	6.84×10^6	1.15×10^3	2×10^3
S2	--	3.6×10^8	200	5	0.014	100	2×10^8	1.36×10^8	5.037×10^5	2×10^3
S3a	1.63×10^9	3.6×10^5	200	5	0.014	100	2×10^8	1.36×10^8	5.037×10^5	2×10^3
S3b,c	1.63×10^9	--	200	5	--	--	2×10^8	1.36×10^8	5.037×10^5	2×10^3
S4a,b,d	1.63×10^9	3.6×10^8	200	5	0.014	100	2×10^8	1.36×10^8	5.037×10^5	2×10^3
S5c,e	1.63×10^9	3.6×10^8	2×10^4	5	0.014	100	2×10^8	1.36×10^8	5.037×10^5	2×10^3
S6	1.63×10^9	3.6×10^8	200	5	0.014	100	2×10^8	1.36×10^8	5.037×10^5	2×10^3
S7	1.63×10^9	3.6×10^8	200	5	0.014	100	2×10^8	1.36×10^8	5.037×10^5	2×10^3
S8	1.63×10^9	3.6×10^8	200	5	0.014	100	2×10^8	1.36×10^8	5.037×10^5	2×10^3
S9	1.63×10^9	3.6×10^8	200	5	0.014	100	2×10^8	1.36×10^8	5.037×10^5	2×10^3
S11	1.63×10^9	3.6×10^8	--	5	0.014	100	2×10^8	1.36×10^8	5.037×10^5	2×10^3
S12	1.63×10^9	3.6×10^9	2×10^4	5	0.014	100	2×10^8	1.36×10^8	5.037×10^5	2×10^3
S13	1.63×10^9	3.6×10^9	2×10^4	5	0.014	100	2×10^8	1.36×10^8	5.037×10^5	2×10^3
S14	1.63×10^9	3.6×10^8	--	5	0.014	100	2×10^8	1.36×10^8	5.037×10^5	2×10^3
S15	2.3×10^9	3×10^8	1×10^5	861	0.075	0.091	2×10^8	3×10^8	9.5×10^{-1}	2×10^3
S16[1]	1×10^9	3×10^9	2039	10.09	0.01**	10**	2×10^8	1.8×10^8	1×10^4	2×10^3
S16[3]	1.8×10^{9}**	3×10^9	180**	0.1234	0.006**	1**	2×10^8	1.4×10^{8}**	999.7	2×10^3
S16[4]	1.9×10^{9}**	3×10^9	207.2	0.01076	0.016**	0.5**	2×10^8	1.88×10^8	1×10^4	2×10^3
S16[5]	1×10^9	2×10^9	1.6×10^4	0.007536	1**	5**	2×10^8	1.8×10^8	1000	2×10^3
S16[6]	1×10^9	3×10^8	2003	153.9	0.005**	0.15**	2×10^8	2×10^8	1000	2×10^3
S16[2]	2.2×10^{9}**	3×10^9	326.8	0.0576	0.015**	0.5**	2×10^8	1.8×10^8	1000	2×10^3
S16[7]	1.4×10^{9}**	3×10^8	1288	2.1	0.038**	0.78**	2×10^8	2×10^8	5.8×10^{-1}	2×10^3

*These parameters are never changed or varied for any simulations

**These parameters were reported by the authors of the experimental data

Bolded figure numbers indicate parameters extracted from the best fits to TTA-UC data

Table S2. Rate parameters used in simulating the effects of sensitizer TTA

	Parameters											
Figure	k_{sens} ($M^{-1}s^{-1}$)	k_{TTA}^{S} ($M^{-1}s^{-1}$)	B_{ISC}	k_{TTA} ($M^{-1}s^{-1}$)	k_T^A (s^{-1})	k_{ex} (cm^2/mJ)	$[S]_0$ (mM)	$[A]_0$ (mM)	k_{IC} (s^{-1})	k_{fl} (s^{-1})	k_{NR} (s^{-1})	k_T^S (s^{-1})
S1a	1.63×10^9	2×10^8	1	3.6×10^8	200	5	--	10	2×10^8	1.36×10^8	5.037×10^5	2×10^3
S1b	1.63×10^5	2×10^8	1	3.6×10^8	200	5	--	10	2×10^8	1.36×10^8	5.037×10^5	2×10^3
S1c	1.63×10^9	2×10^8	1	--	200	5	0.014	10	2×10^8	1.36×10^8	5.037×10^5	2×10^3
S1d	1.63×10^9	2×10^8	1	3.6×10^4	200	5	0.014	10	2×10^8	1.36×10^8	5.037×10^5	2×10^3

Table S3. Summary of the MATLAB code available on Github: https://github.com/kabhi17/TTA-model.git

File name	Content and purpose
'FssShow.m'	Simulating logarithmic F_{SS} vs. I curves
'LocalSlopeShow.m'	Computing $n(I)$ and calculating irradiance values for specific values of n
'TWShow.m'	Calculating Γ and the analytical quantity $\log(I_{sat}/I_{th})$
'QYShow.m'	Calculating values of Φ_{UC} and $\Phi_{UC,max}$
'FittingShow.m'	Preparing experimental data for fitting

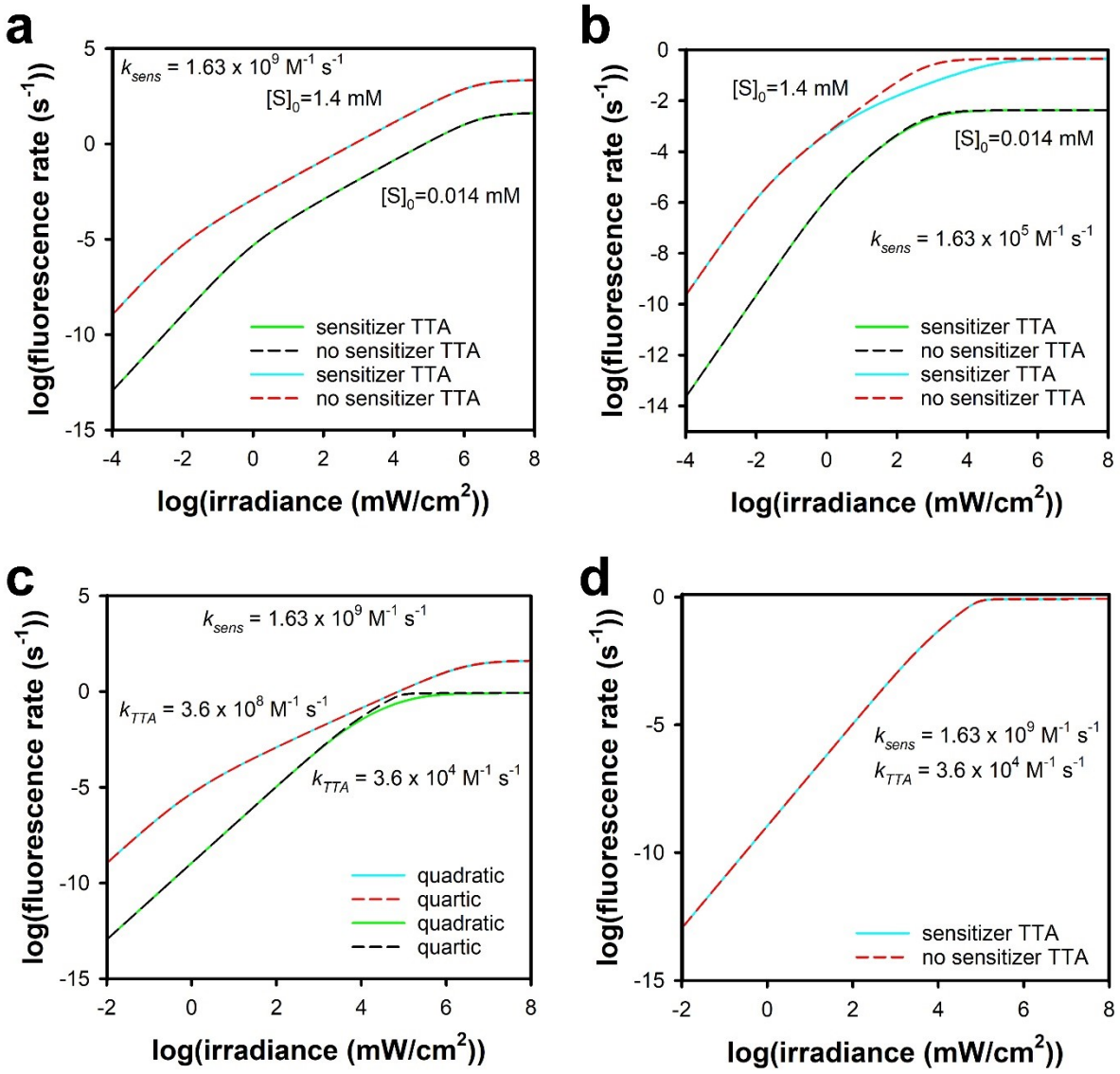

Fig. S1 Exploring the influence of sensitizer TTA. (a) Log-log plot of fluorescence versus irradiance with sensitizer TTA events included (solid lines) and excluded (dashed lines) for $[S]_0$ = 0.014 mM (A) and for $[S]_0$ = 0.14 mM. Here $k_{sens} = 1.63 \times 10^9$ M^{-1} s^{-1}. (b) Same as (a), except $k_{sens} = 1.63 \times 10^5$ M^{-1} s^{-1}. (c) Log-log plot of fluorescence versus irradiance for the quartic (solid lines) and quadratic (dashed lines) model for different annhilator TTA rate constants. (d) Log-log plot of fluorescence versus irradiance for the quartic model, with sensitizer TTA events included (solid line) and excluded (dahsed line).

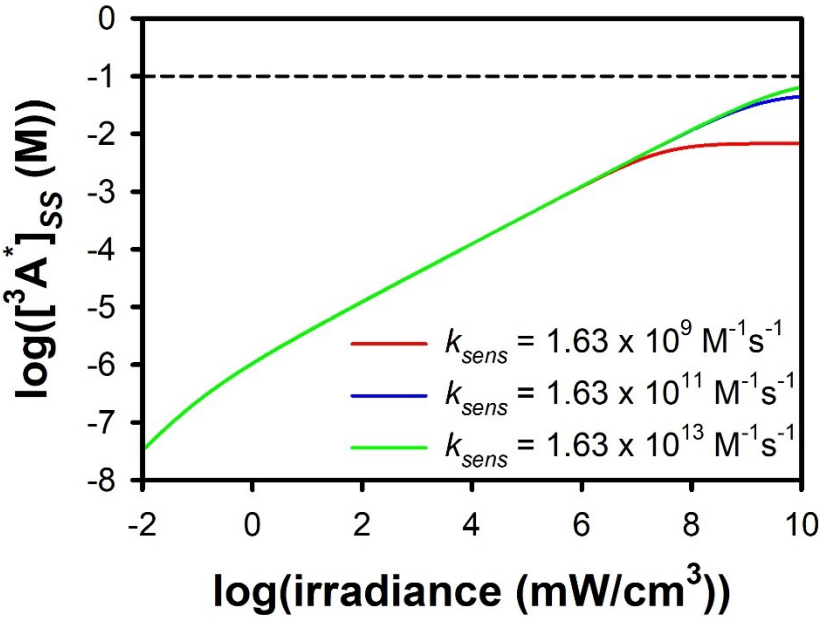

Fig. S2 The dependence of the steady-state annihilator triplet concentration $[^3A^*]_{SS}$ on irradiance for different values of k_{sens}. The values of all of the other parameters are given in Table S1. The dashed line indicates the value of $[A]_0$.

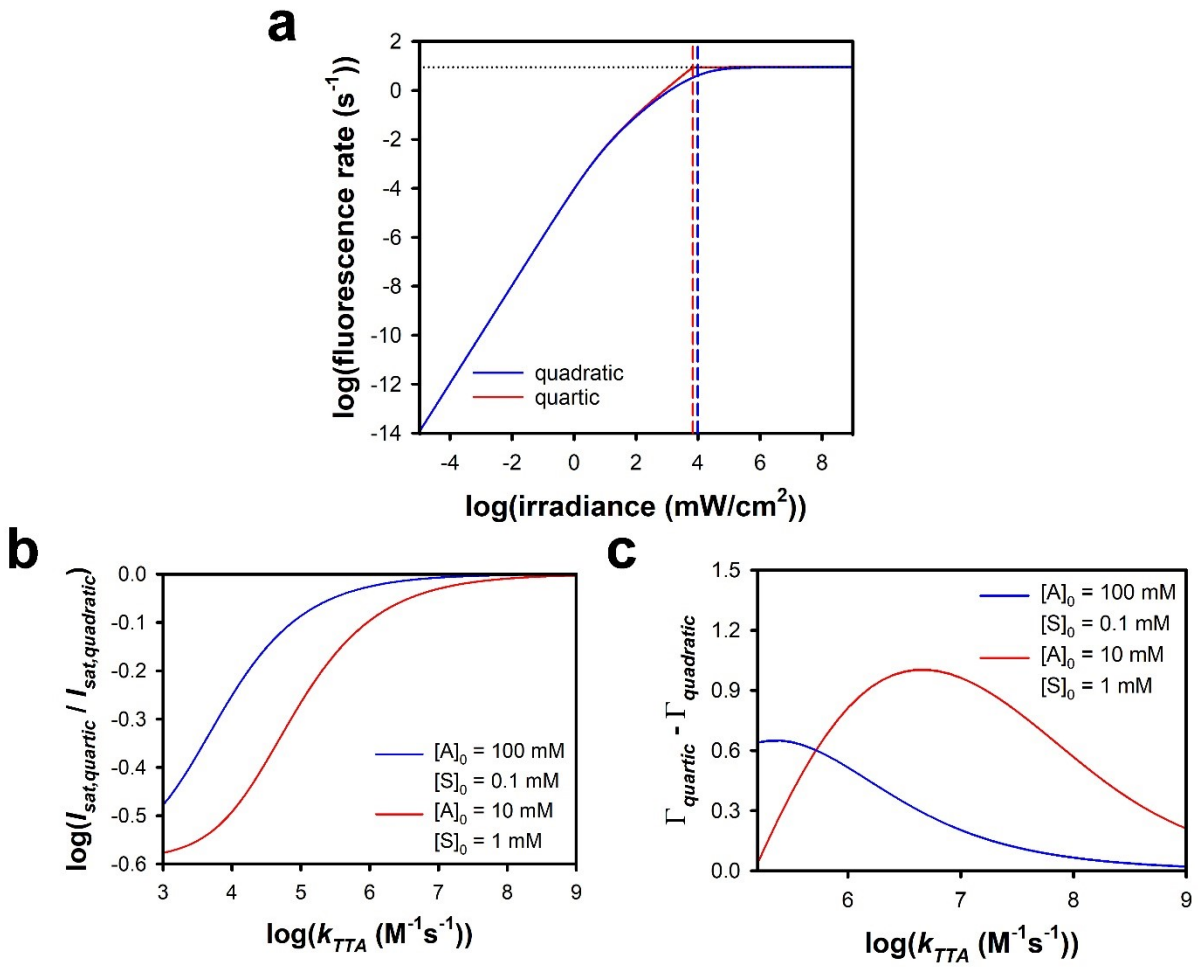

Fig. S3 Comparison of saturation in the quadratic and quartic models. (a) Representative TTA-UC curves in the quadratic (blue) and quartic (red) models. The dashed lines of the corresponding colors indicate the value of I_{sat}. The dotted line is the saturation level of fluorescence. (b) Logarithm of the ratio of the saturation irradiance as a function of k_{TTA} in the quartic model to that in the quadratic model for two different sets of annihilator and sensitizer concentrations. The quartic model always saturates at a lower irradiance. (c) The value of Γ as a function of k_{TTA} in the quartic model minus that in the quadratic model for two different sets of annihilator and sensitizer concentrations. In this region of the parameter space, the transition width in the quartic model is larger than that in the quadratic model. See Table S1 for the values of the other parameters.

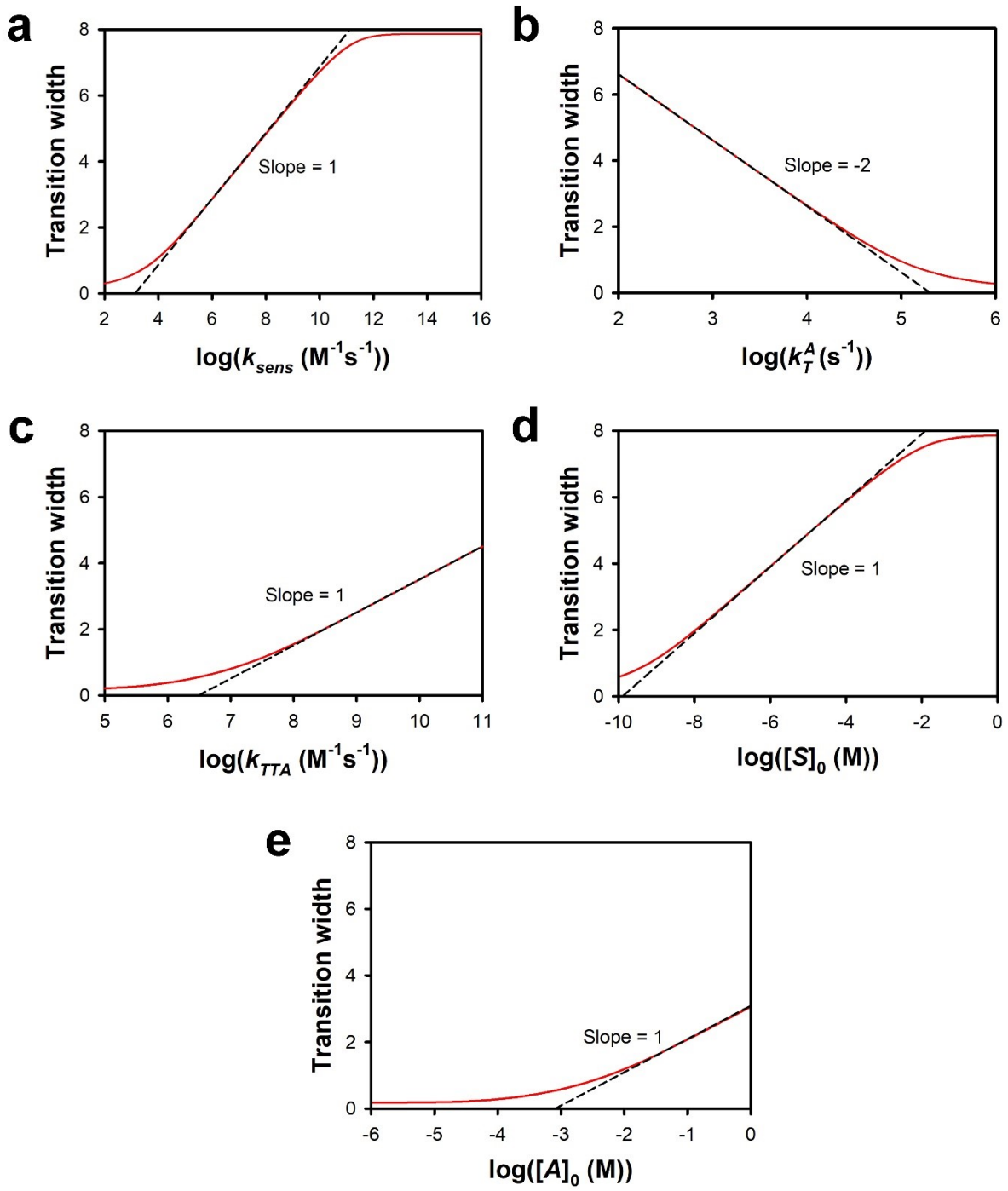

Fig. S4 The dependence of the transition width, Γ, on (a) k_{sens}, (b) k_T^A, (c) k_{TTA}, (d) $[S]_0$, and (e) $[A]_0$. The values of all other parameters are given in Table S1. The dashed lines are guides for the eye.

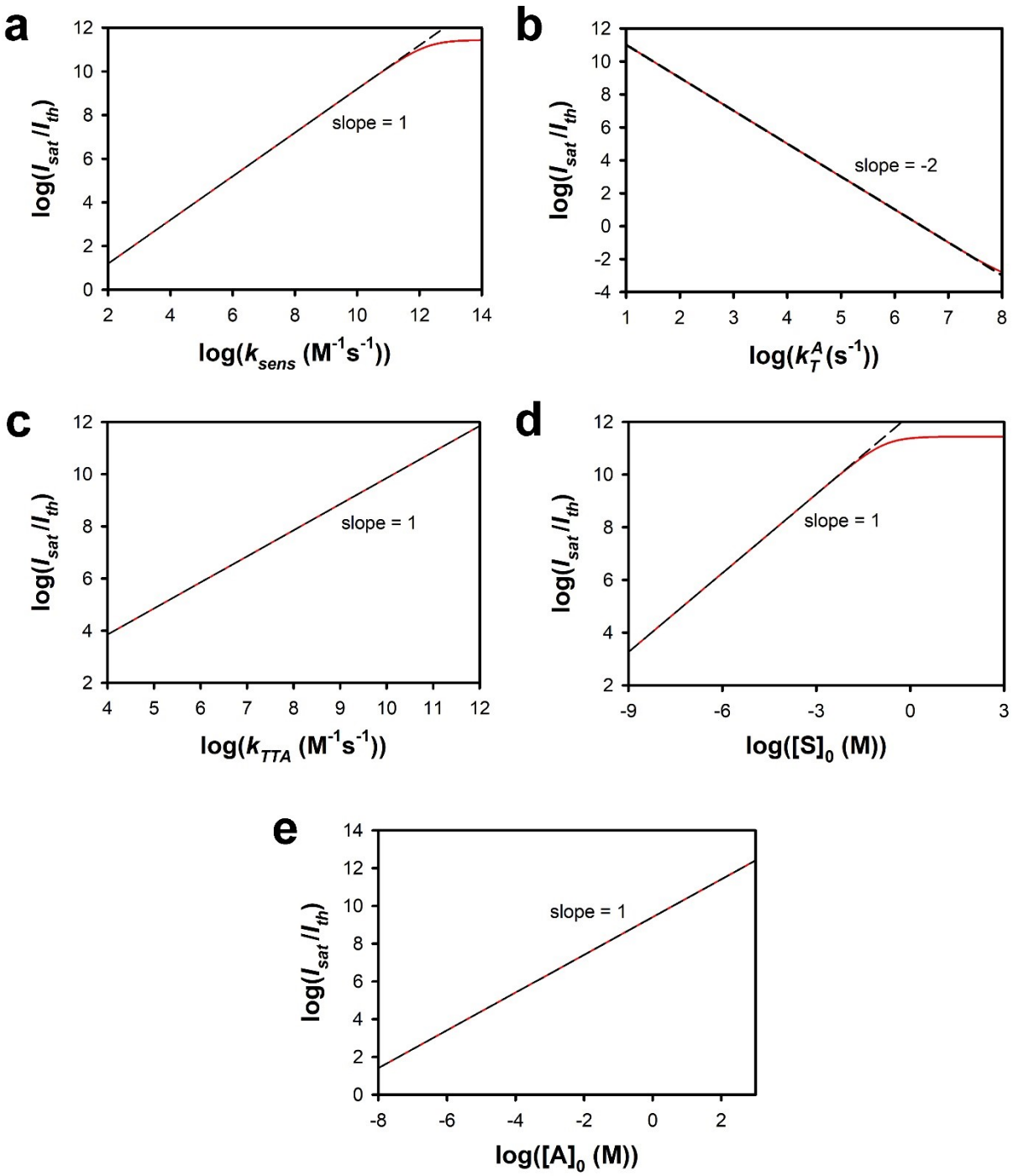

Fig. S5 The dependence of $\log(I_{sat}/I_{th})$ on (a) k_{sens}, (b) k_T^A, (c) k_{TTA}, (d) $[S]_0$, and (e) $[A]_0$. The values of all other parameters are given in Table S1. The dashed lines are guides for the eye.

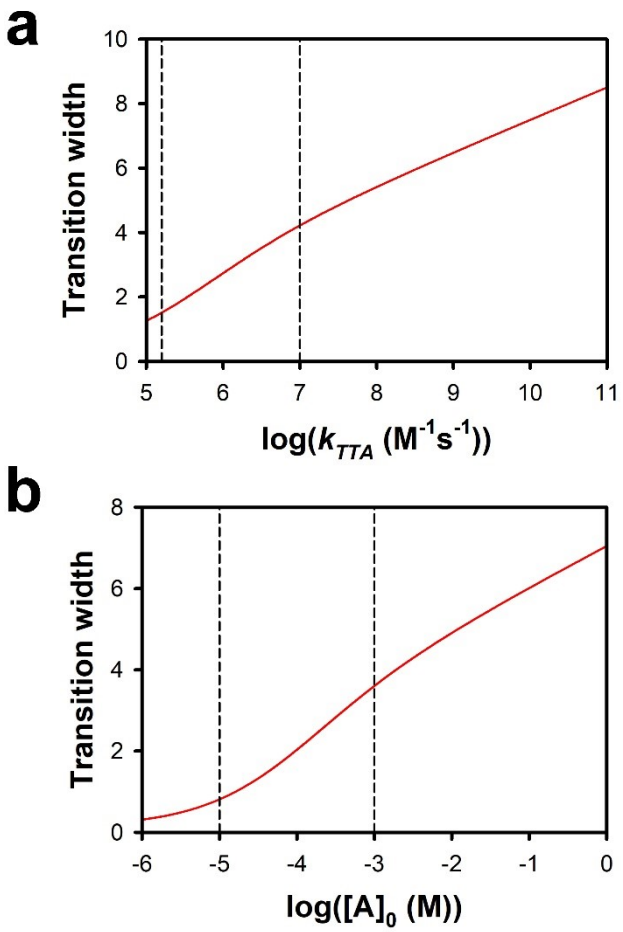

Fig. S6 The dependence of the transition width, Γ, on (a) the rate constant k_{TTA} and (b) the annihilator concentration $[A]_0$. The values of all of the other parameters are given in Table S1. Within the regions between the dashed lines, $\Gamma \propto (k_{TTA})^{1.6}$.

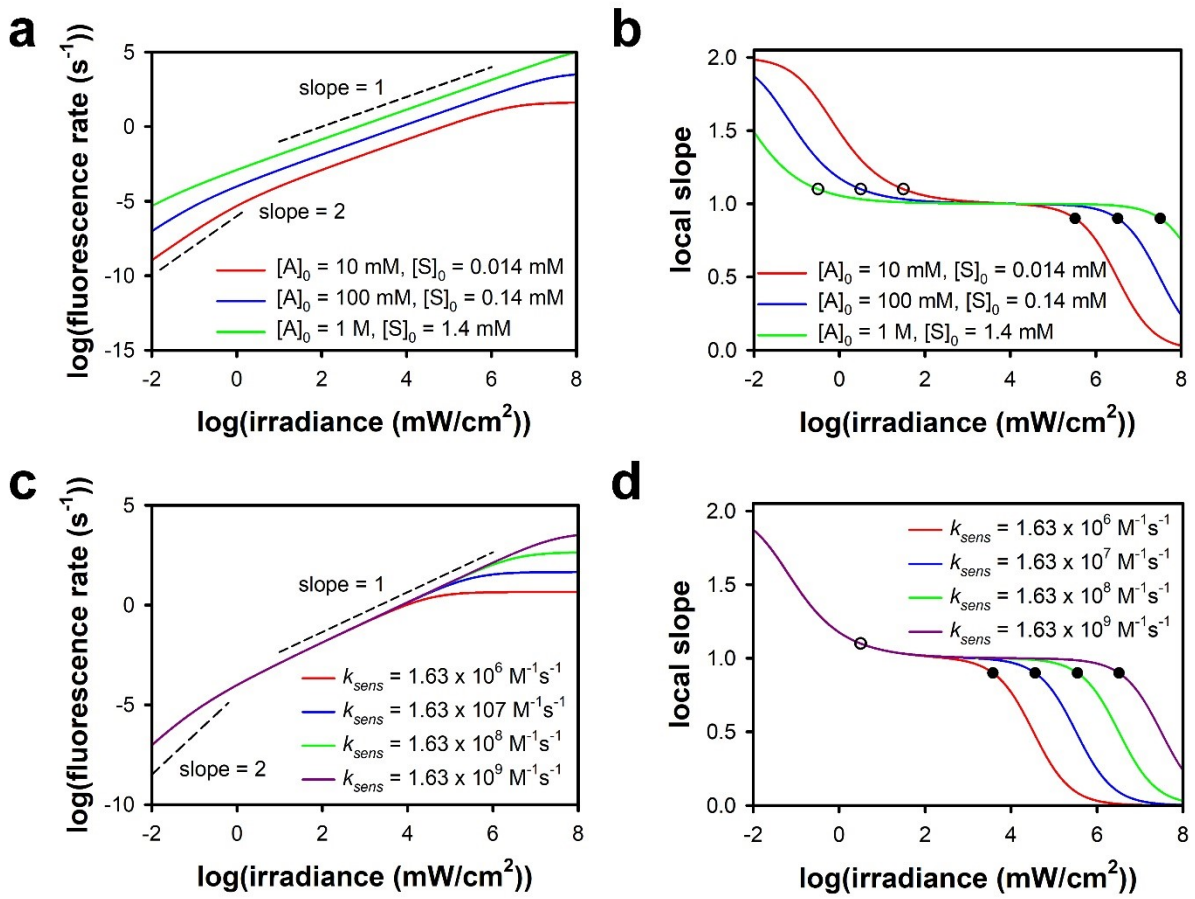

Fig. S7 The dependence of the upconversion quantum yield and its slope on irradiance for (a) and (b), respectively, different combinations of values of $[A]_0$ and $[S]_0$, and (c) and (d), respectively, different values of k_{sens}. The open and filled circles indicate the irradiances at which the local slope is 1.1 and 0.9, respectively. See Table S1 for the values of the other parameters.

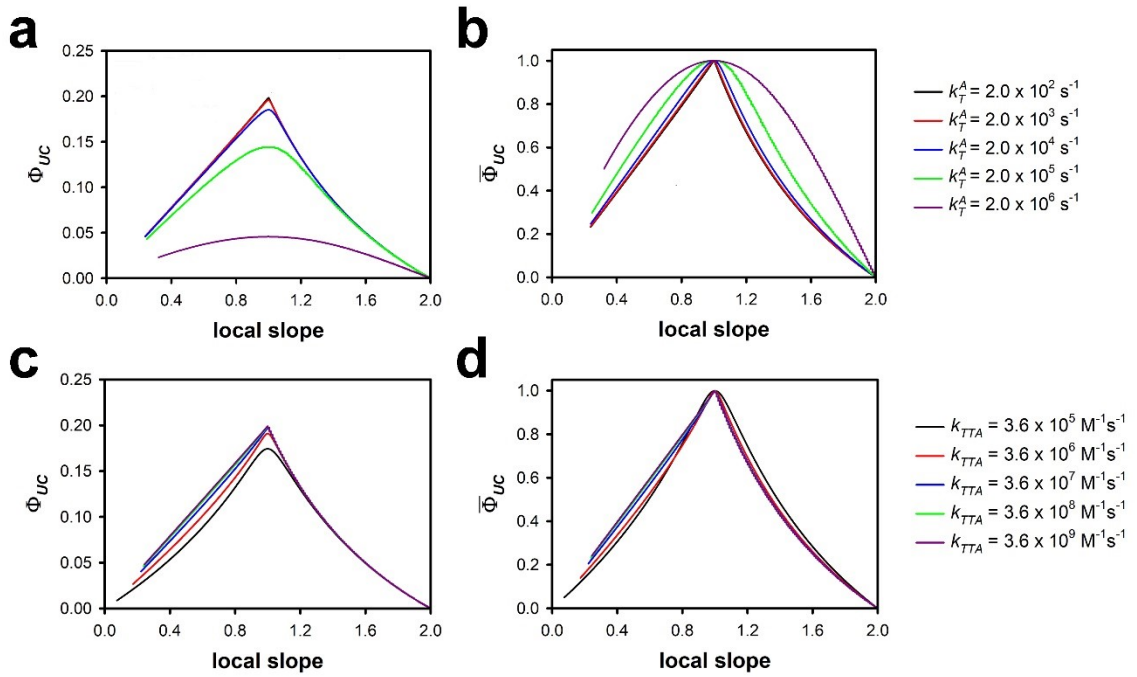

Fig. S8 (original) The dependence of the upconversion quantum yield and the normalized upconversion quantum yield on the local slope *n* for (a) and (b), respectively, different values of k_T^A, and (c) and (d), respectively, different values of k_{TTA}. The quantum yield always increases monotonically with the local slope until that slope attains a value of 1, after which the quantum yield decreases. See Table S1 for the values of the other parameters.

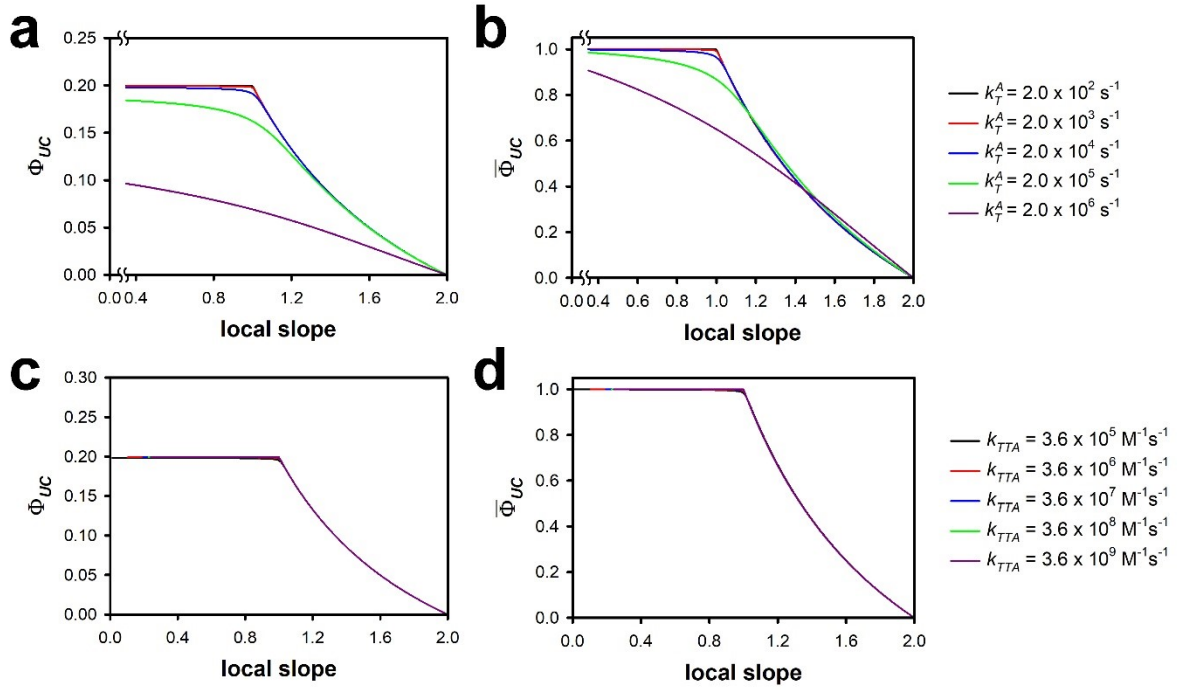

Fig. S8 (corrected) The dependence of the upconversion quantum yield and the normalized upconversion quantum yield on the local slope *n* for (a) and (b), respectively, different values of k_T^A, and (c) and (d), respectively, different values of k_{TTA}. The quantum yield always increases monotonically with the local slope until that slope attains a value of 1, at which point the quantum yield begins to saturate. See Table S1 for the values of the other parameters.

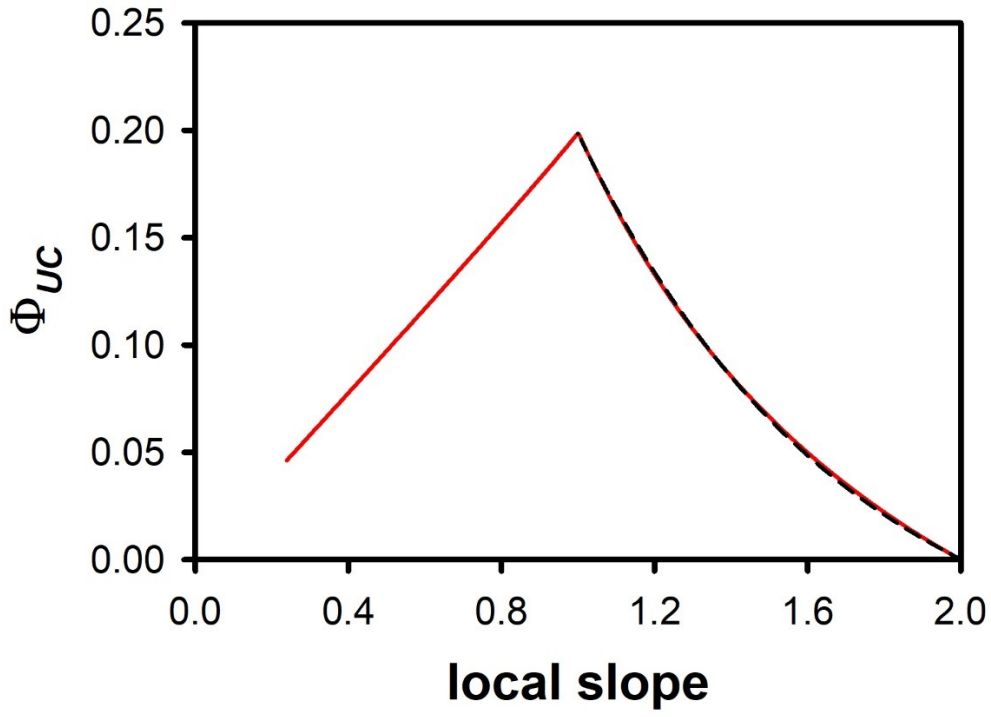

Fig. S9 (original) An empirical fit of the dependence of the upconversion quantum yield on the local slope to eqn (37) for n values ≥ 1.

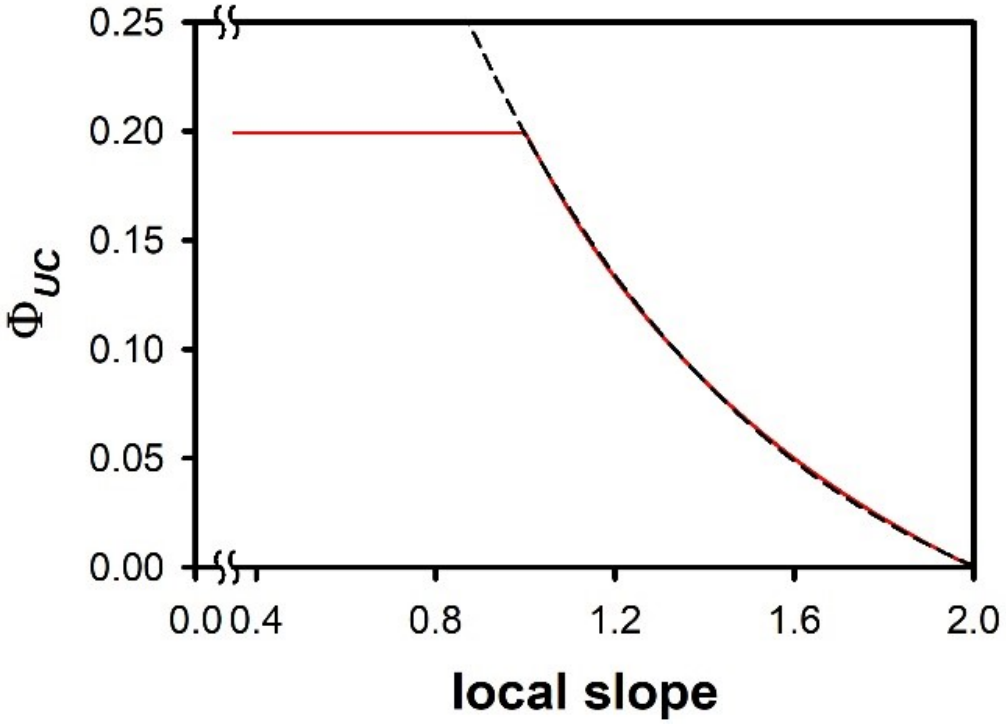

Fig. S9 (corrected) An empirical fit of the dependence of the upconversion quantum yield on the local slope to eqn (37) for n values ≥ 1.

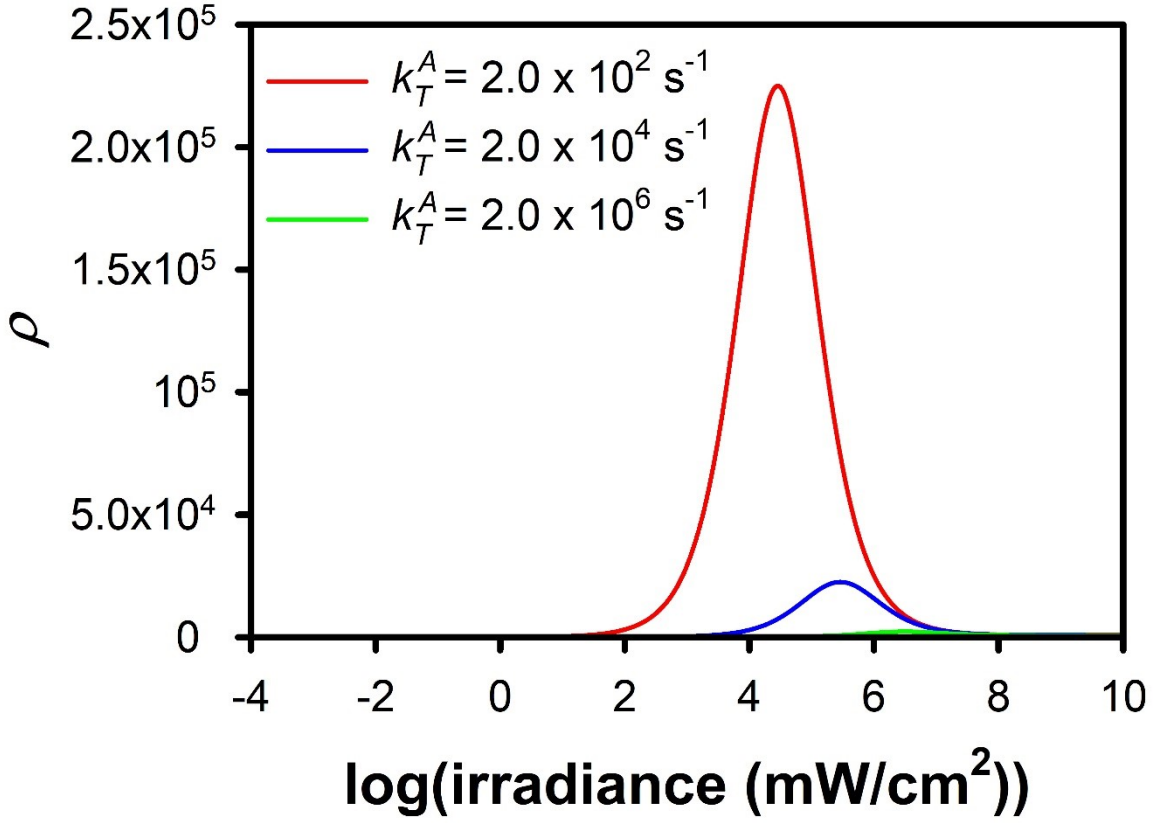

Fig. S10 The dependence of ρ, the second term in the radicand in eqn (14), on irradiance for different values of k_T^A. See Table S1 for the values of the other parameters.

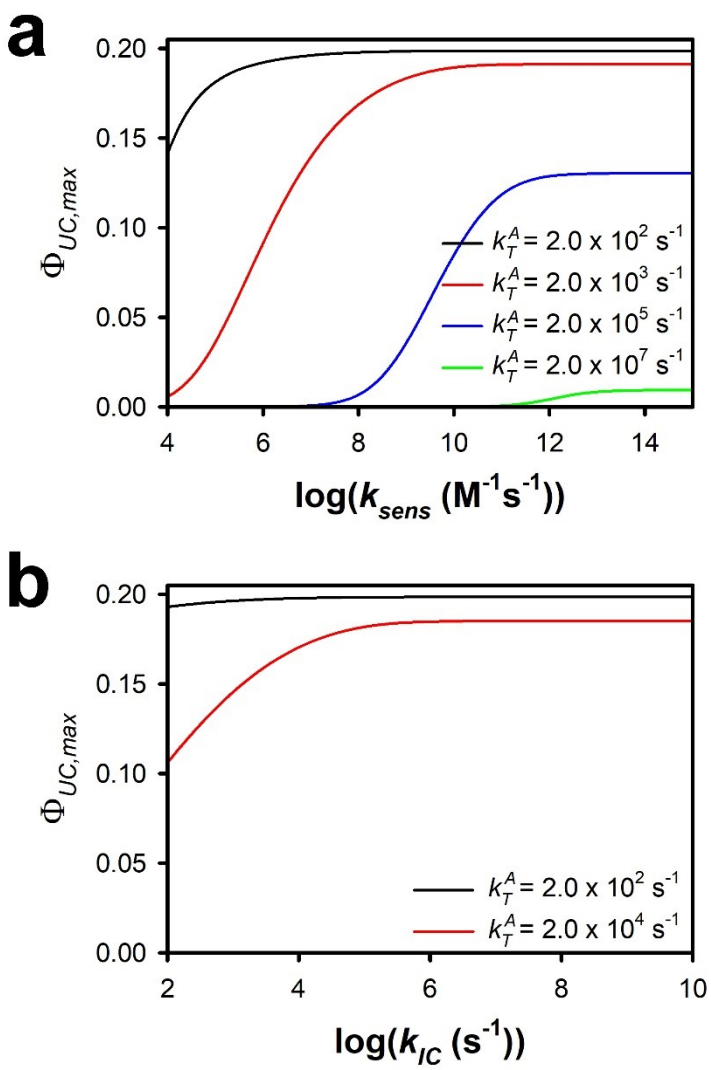

Fig. S11 (original) The dependence of the maximum upconversion quantum yield on (a) k_{sens} and (b) k_{IC} for several values of k_T^A. See Table S1 for the values of the other parameters.

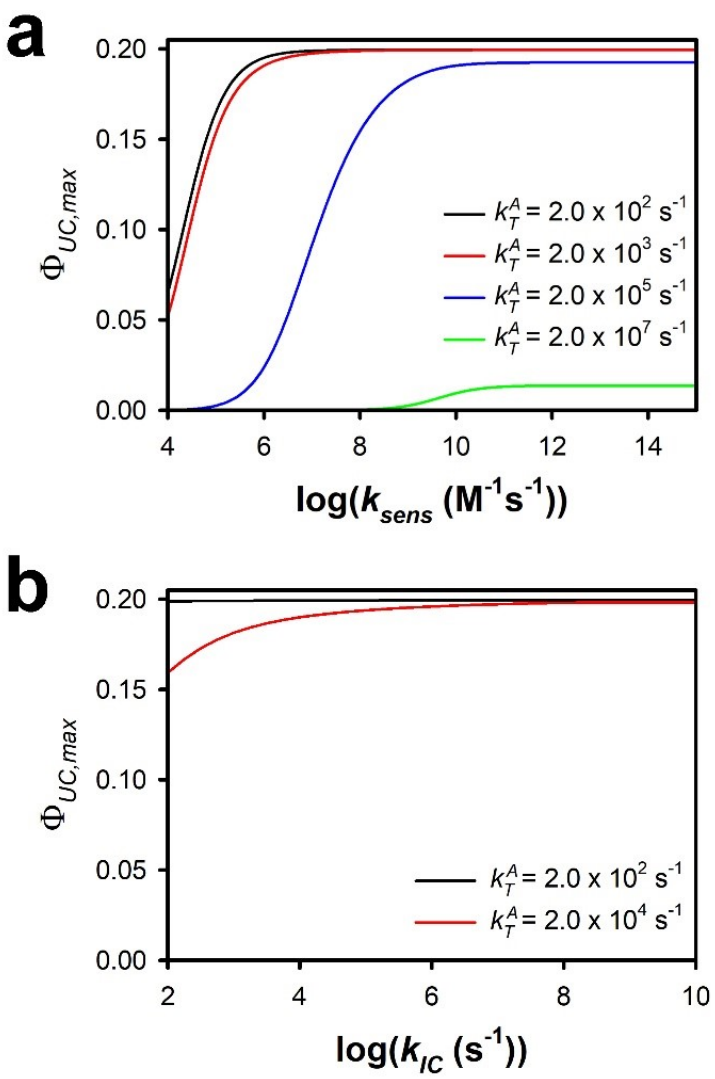

Fig. S11 (corrected) The dependence of the maximum upconversion quantum yield on (a) k_{sens} and (b) k_{IC} for several values of k_T^A. See Table S1 for the values of the other parameters.

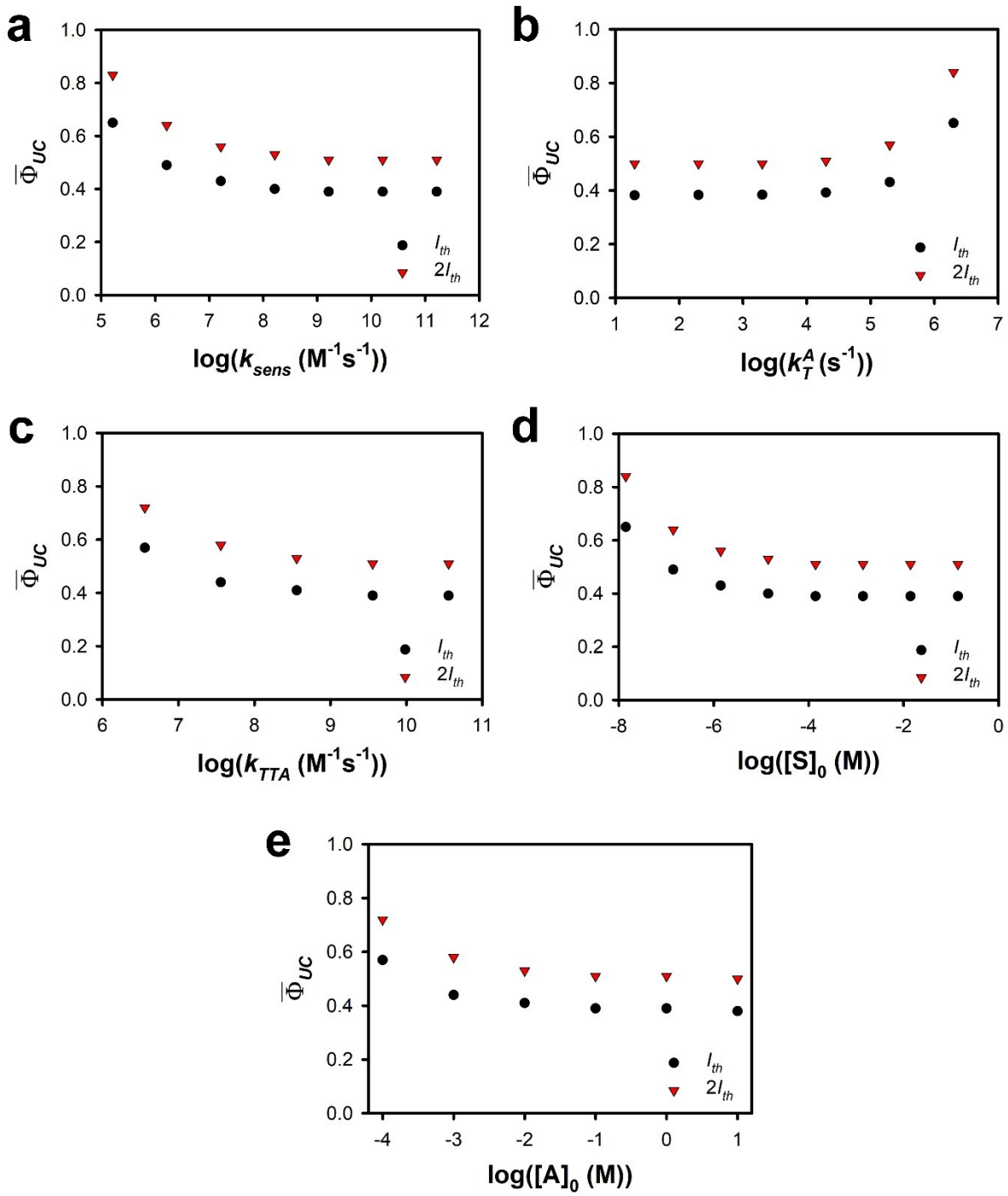

Fig. S12 (original) The normalized upconversion quantum yield at irradiances I_{th} and $2I_{th}$ as a function of (a) k_{sens}, (b) k_T^A, (c) k_{TTA}, (d) $[S]_0$, and (e) $[A]_0$. See Table S1 for the values of the other parameters.

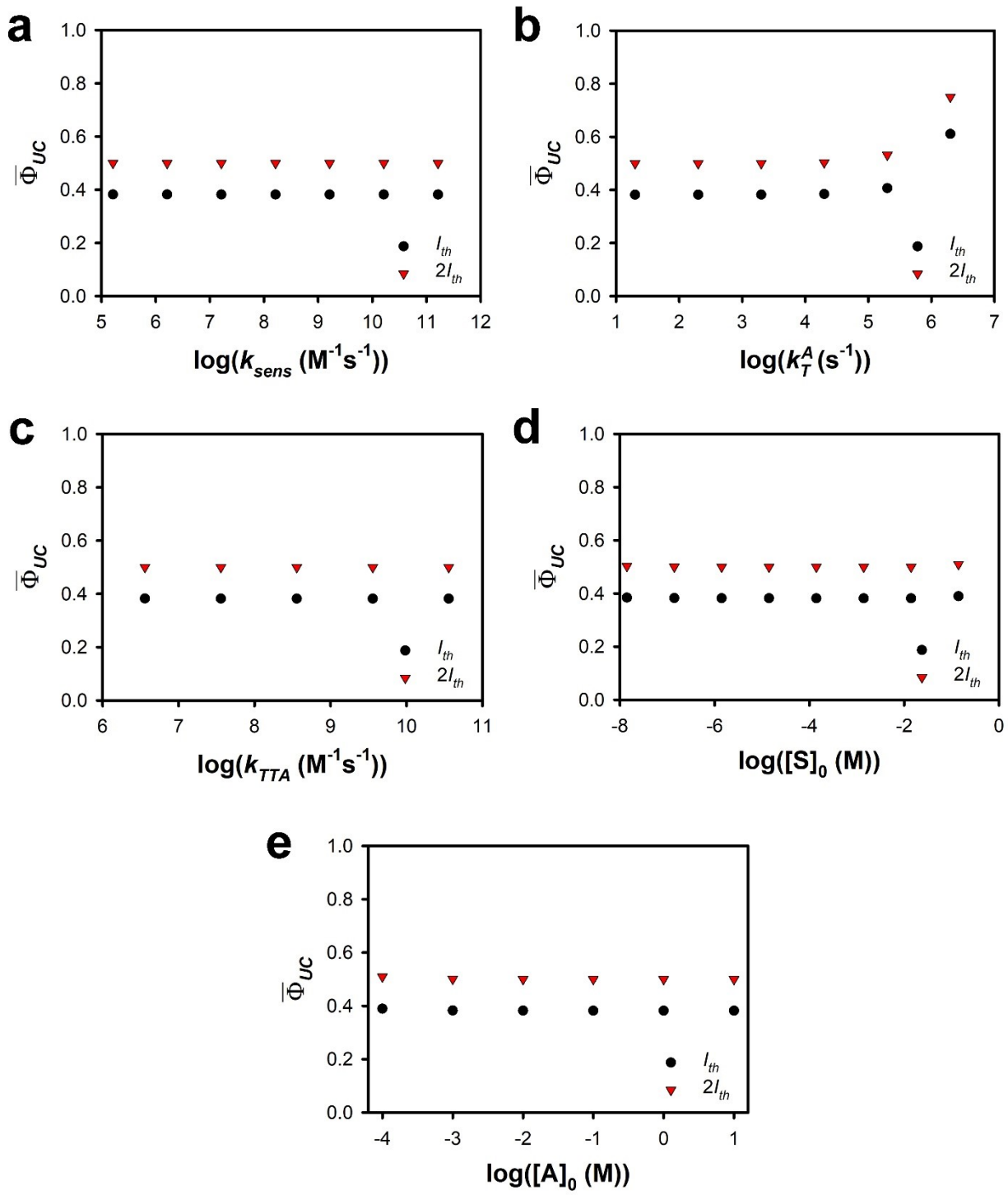

Fig. S12 (corrected) The normalized upconversion quantum yield at irradiances I_{th} and $2I_{th}$ as a function of (a) k_{sens}, (b) k_T^A, (c) k_{TTA}, (d) $[S]_0$, and (e) $[A]_0$. See Table S1 for the values of the other parameters.

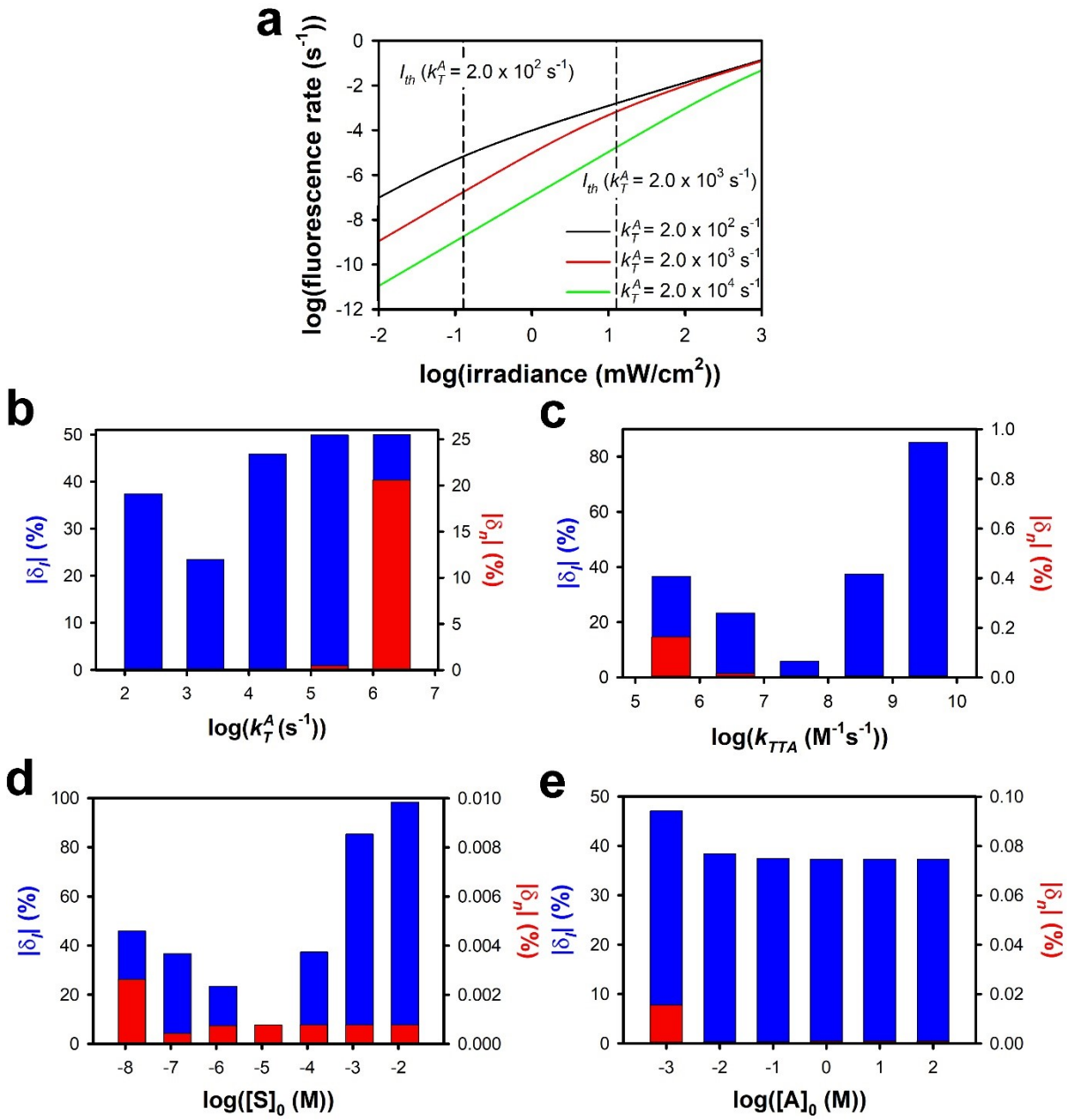

Fig. S13 (a) Representative calculated TTA-UC curves for different values of k_T^A, along with I_{th} values. In the case of the highest value of k_T^A, I_{th} is outside of the range of irradiances. Predicted errors in I_{th} and $n(I_{th})$ for different values of (b) k_T^A, (c) k_{TTA}, (d) $[S]_0$, and (e) $[A]_0$. See Table S1 for the values of the other parameters.

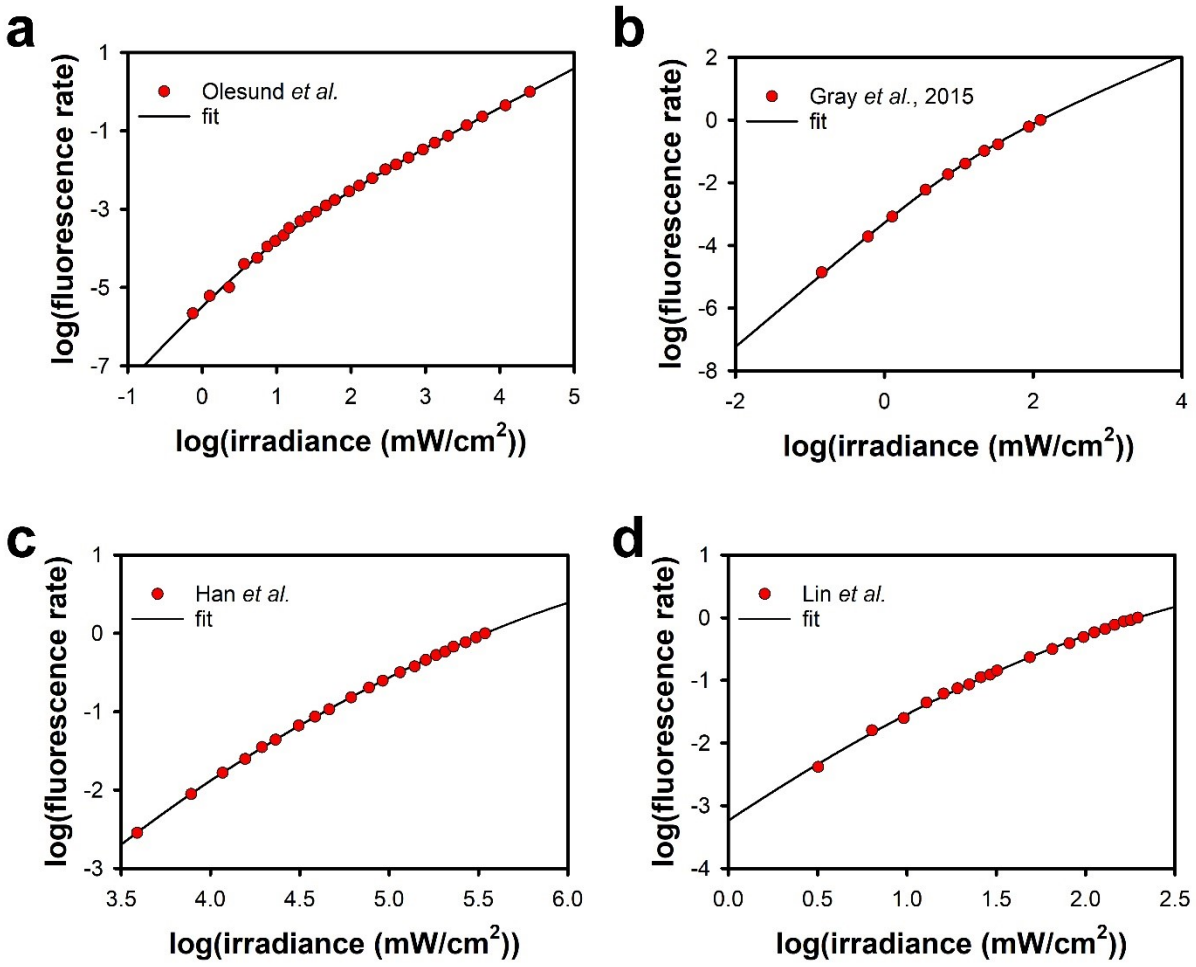

Fig. S14 Fits of the quadratic model (solid line) to literature TTA-UC data in solution (symbols) from (a) Olesund *et al.*[3], (b) Gray *et al.*[2], (c) Han *et al.*[6], and (d) Lin *et al.*[6]

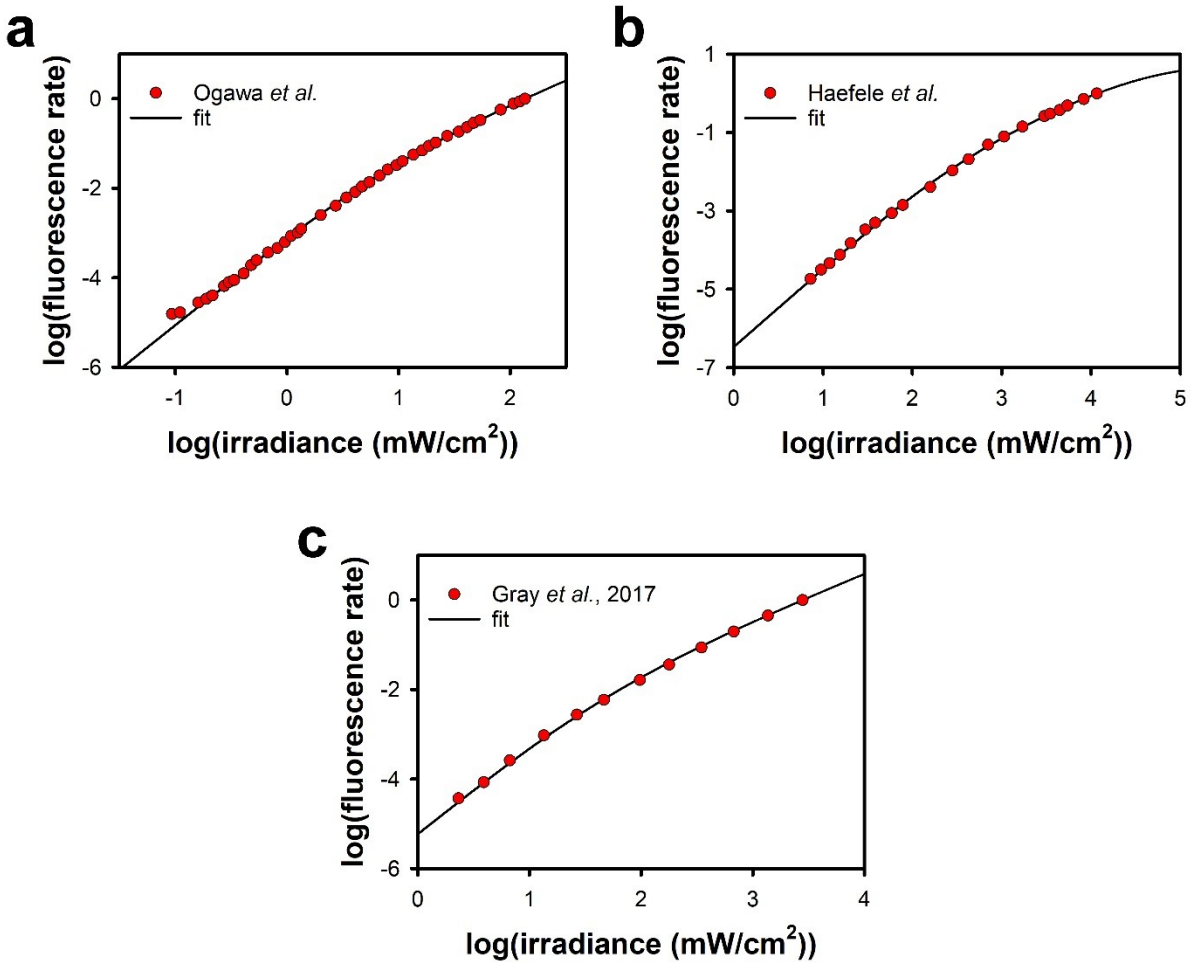

Fig. S15 Fits of the quadratic model (solid line) to literature TTA-UC data in solution (symbols) from (a) Ogawa *et al.*[1], (b) Haefele *et al.*[7], and (c) Gray *et al.*[4]

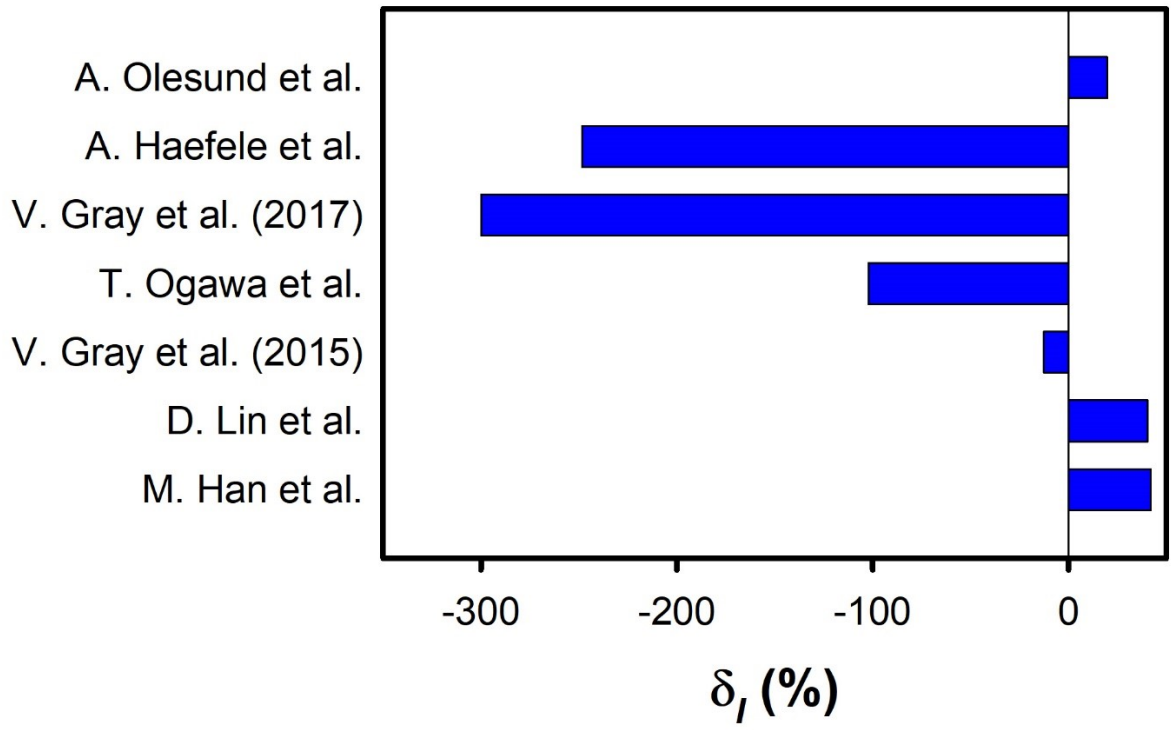

Fig. S16 Values of $\delta_I = \frac{I_{th,fit} - I_{th,reported}}{I_{th,fit}} \cdot 100\%$ for the experimental data in Figs. S14 and S15.

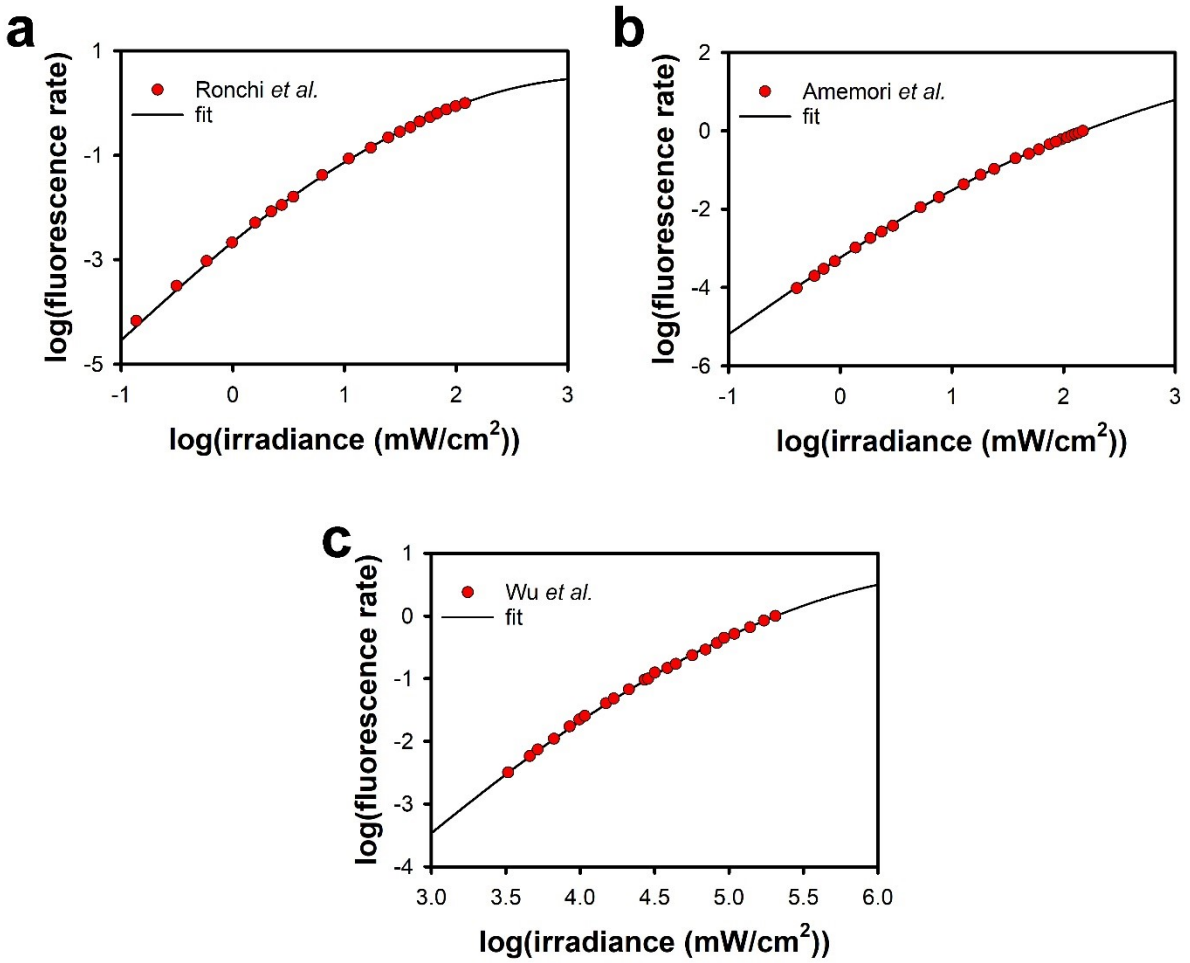

Fig. S17 Fits of the quadratic model (solid line) to literature TTA-UC data (symbols) for (a) nanocrystal-sensitized systems,[8] and (b) and (c) upconverting core/shell nanoparticles.[9, 10]

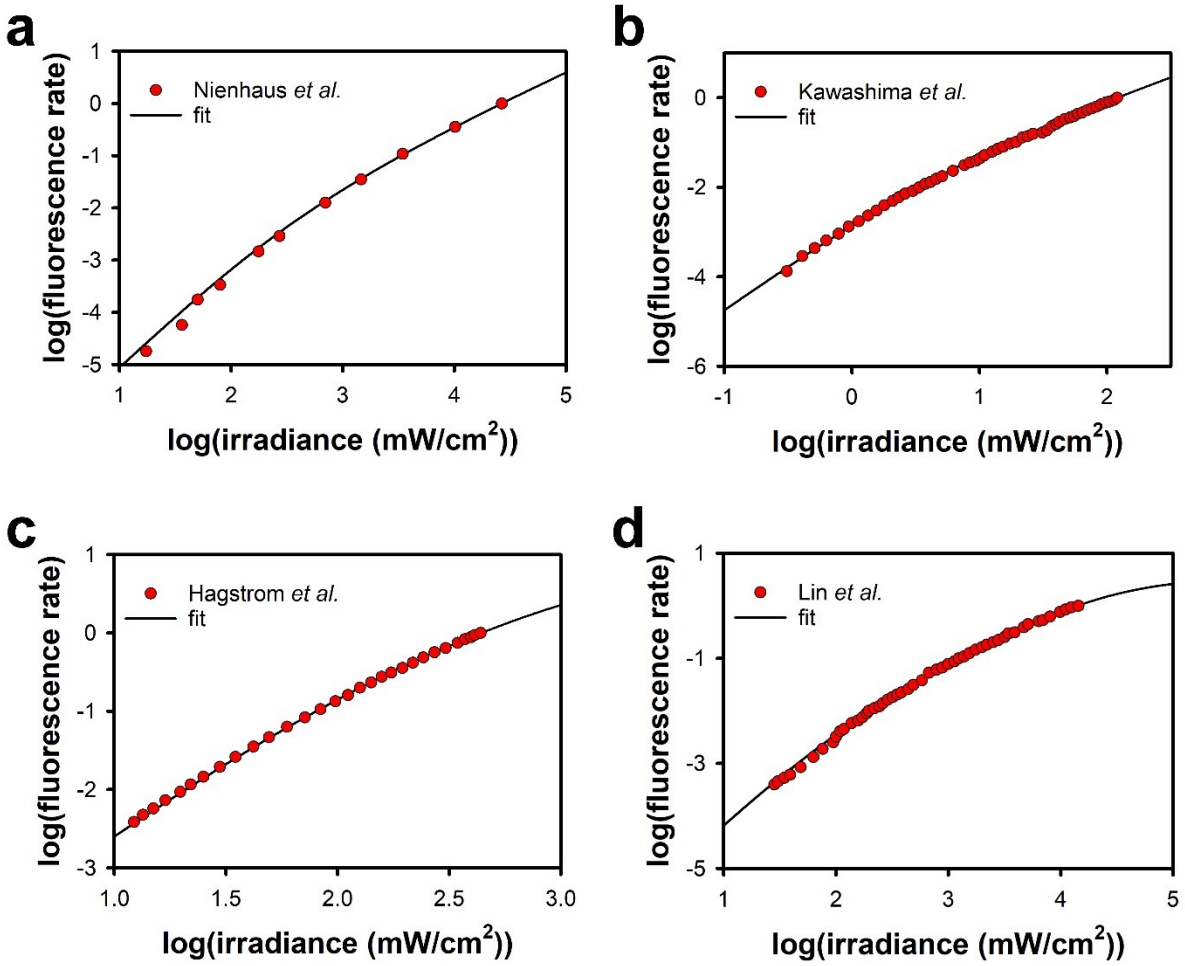

Fig. S18 Fits of the quadratic model (solid line) to literature TTA-UC data (symbols) for (a) perovskite-sensitized annihilator/acceptor solid films,[11] (b) dispersed sensitizer/annihilator assemblies,[12] and (c) and (d) spin-coated thin films.[13, 14]

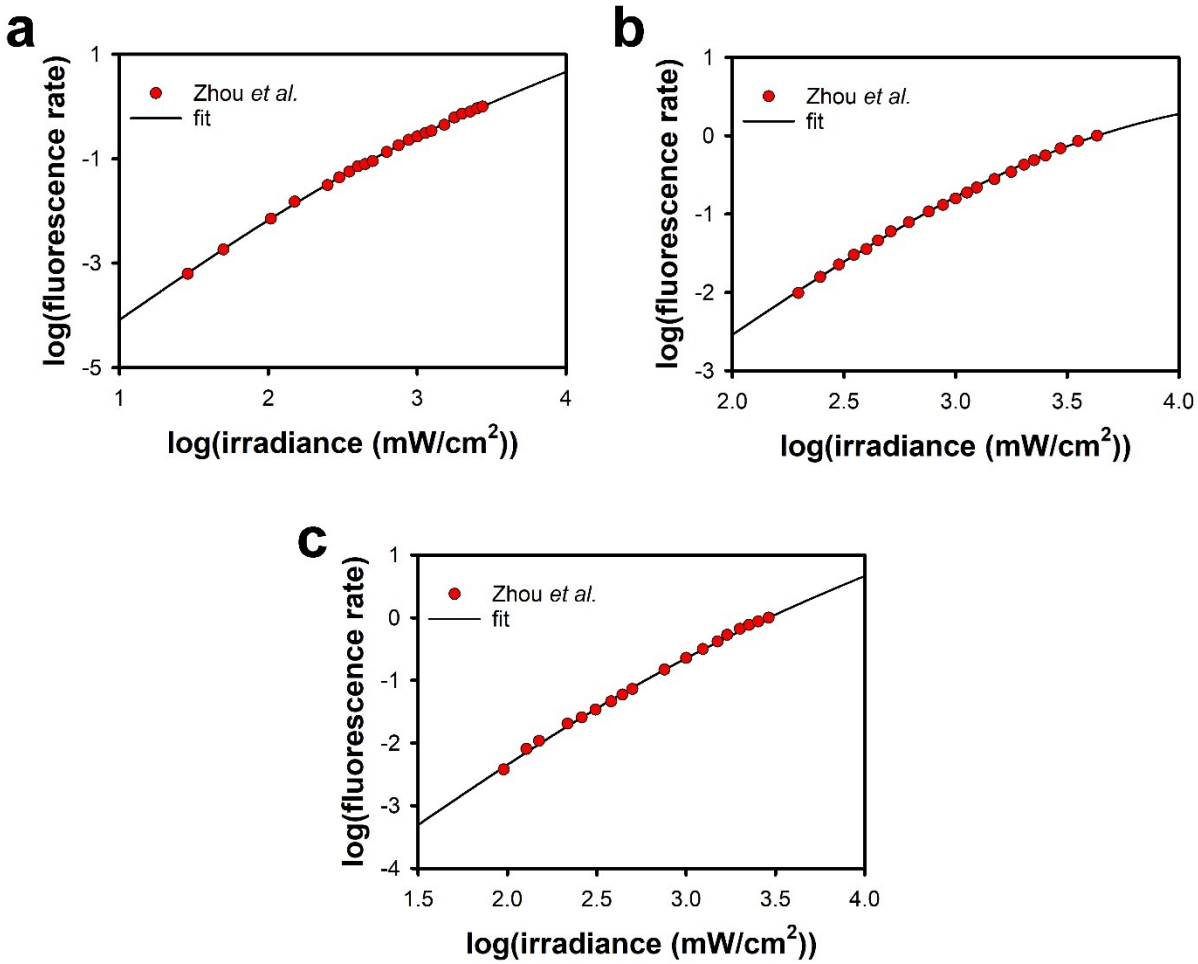

Fig. S19 Fits of the quadratic model (solid line) to literature TTA-UC data (symbols) for self-assembled layers for acceptors (a) **1**, (b) **2**, and (c) **3** from Zhou *et al.*[15] Note that the two data points at the lowest irradiances in (a) were not in the original paper.

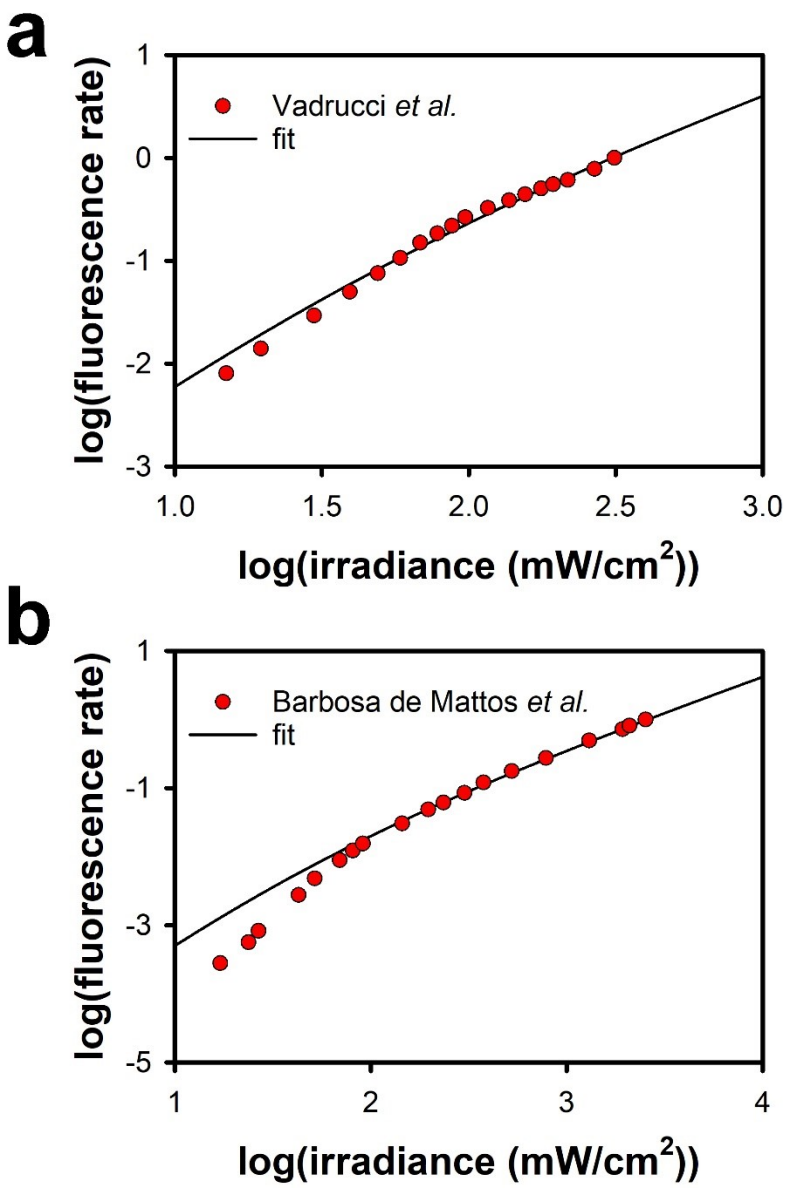

Fig. S20 Fits of the quadratic model (solid line) to literature TTA-UC data (symbols) for the gel-based systems of (a) Vadrucci *et al*.[16] and (b) Barbosa de Mattos *et al*.[17]

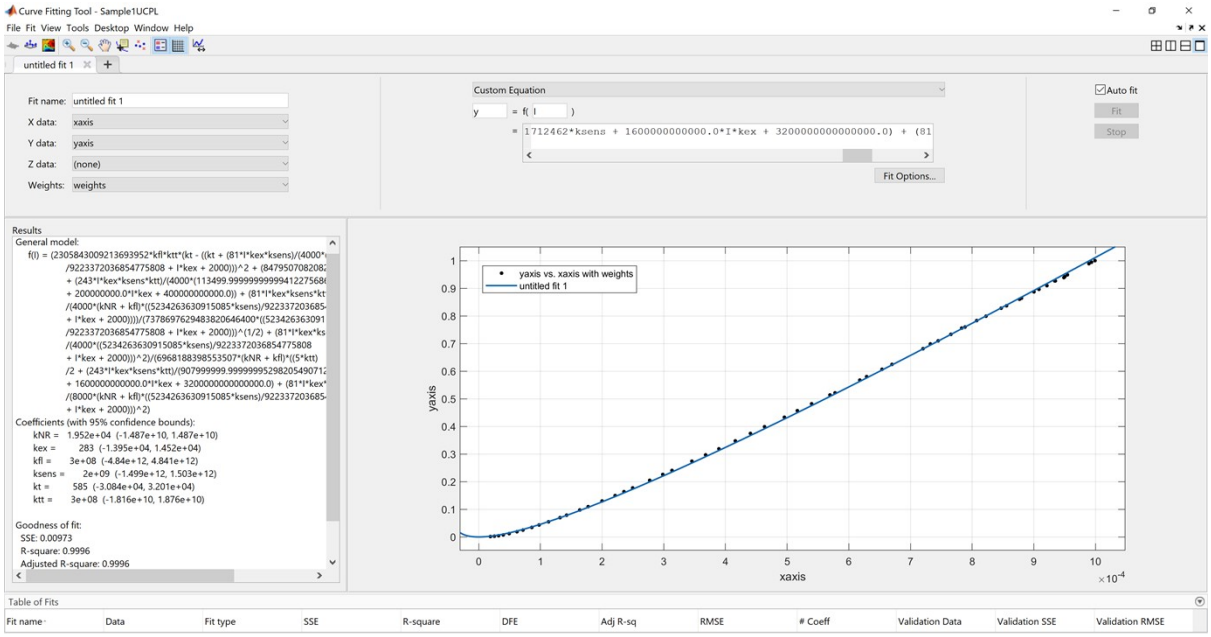

Fig. S21 An example of curve fitting being performed on experimental TTA-UC data. Note that the linear data is being fit, not the logarithmic data. The rate constants obtained from the fit are shown in the 'Results' box.

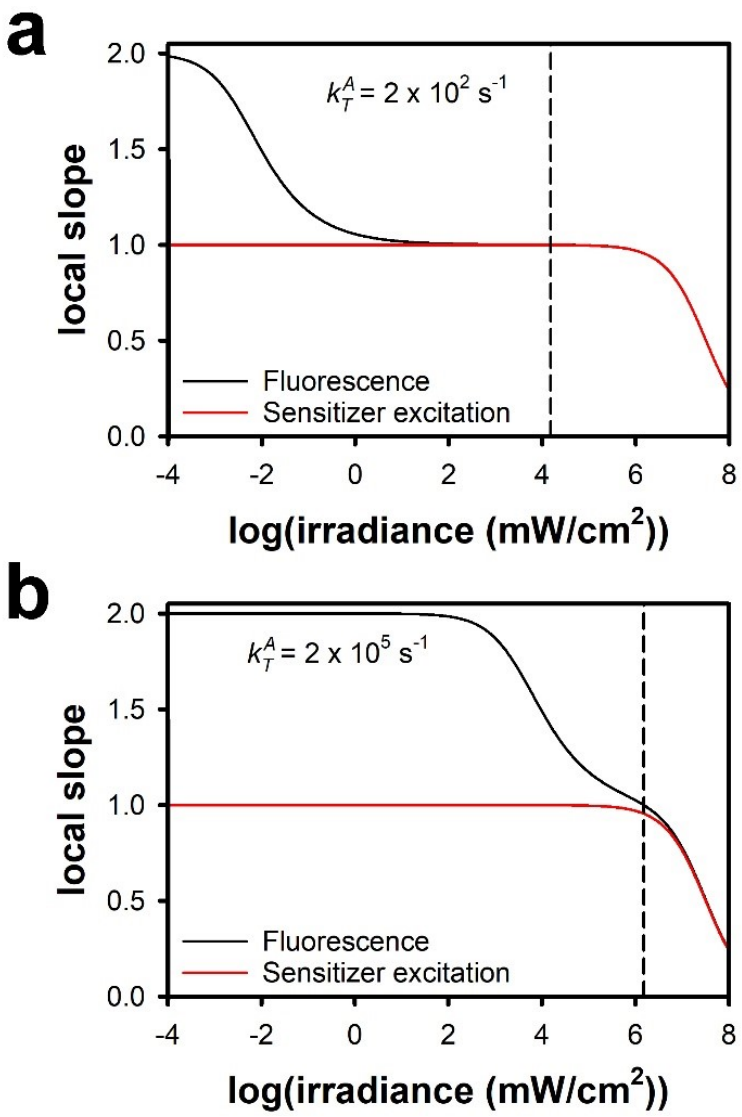

Fig. S22 Local slopes of the rates of annihilator fluorescence, $n(I)$ (black) and sensitizer excitation, $q(I)$, (red) as a function of irradiance for (a) $k_T^A = 2 \times 10^2\ s^{-1}$ and (b) $k_T^A = 2 \times 10^5\ s^{-1}$. The values for all other rate parameters are the same as for Figs. 3, 4, 5, 6, and 7 (See Table S1). The vertical dashed lines indicate the irradiance at which $n(I) = 1$.